available at www.sciencedirect.com

SCIENCE DIRECT®

www.elsevier.com/locate/brainres

ELSEVIER

BRAIN RESEARCH

Research Report

Altered glycosylation of α-dystroglycan in neurons of Fukuyama congenital muscular dystrophy brains

Yoshiaki Saito[a,b,*], *Tomoko Yamamoto*[c], *Masashi Mizuguchi*[d], *Makio Kobayashi*[c], *Kayoko Saito*[a], *Kousaku Ohno*[b], *Makiko Osawa*[a]

[a]*Department of Pediatrics, Tokyo Women's Medical University, Japan*
[b]*Division of Child Neurology, Institute for Neurological Sciences, Tottori University, Japan*
[c]*Department of Pathology, Tokyo Women's Medical University, Japan*
[d]*Department of Pediatrics, Tokyo University, Japan*

ARTICLE INFO

Article history:
Accepted 27 December 2005
Available online 7 February 2006

Keywords:
α-Dystroglycan
Fukutin
Fukuyama congenital muscular dystrophy
Glycosylation
Glia-limitans

Abbreviations:
FCMD, Fukuyama congenital muscular dystrophy
α-DG, α-dystroglycan

ABSTRACT

To test the hypothesis that the disruption of fukutin protein produces the brain pathology through hypoglycosylation of α-dystroglycan (α-DG), we immunostained Fukuyama congenital muscular dystrophy (FCMD) brains with an antibody that recognizes the polysaccharide epitope of α-DG. Immunoreactivity of the glia-limitans along the cortical surface, as well as that of the glial endfeet around vessel walls, was preserved in the FCMD cerebrum. However, fragmentation of the immunostained glia-limitans was noted in association with parenchymal protrusion and gyral fusion. In the FCMD cerebellum, this fragmentation of α-DG labeling was limited to the area of micropolygyria, and immunostaining at the glia-limitans and vessel walls was comparable to that of the control brains, in structurally normal areas. In the hippocampus, neurons of the dentate gyrus and corpus ammonis were immunopositive for α-DG in control subjects, but this staining was markedly decreased in FCMD brains. In contrast, immunolabeling of blood vessels and the glia-limitans was preserved in this region. Fukutin antisera clearly labeled hippocampal neurons in control brains, while this labeling was decreased in FCMD brains. Thus, hypoglycosylation of α-DG was evident in neurons, but not in the glial cell population of FCMD brains. This suggests that the mechanism of α-DG glycosylation may differ between neurons and glial cells, and that a fukutin gene defect may result in functional disruption through hypoglycosylation of both neuronal and glial α-DG.

* *Corresponding author.* Division of Child Neurology, Institute for Neurological Sciences, Tottori University, 36-1 Nishi-cho, Yonago 683-8504, Japan. Fax: +81 859 38 6779.
E-mail address: saitoyo@grape.med.tottori-u.ac.jp (Y. Saito).

0006-8993/$ – see front matter © 2006 Elsevier B.V. All rights reserved.
doi:10.1016/j.brainres.2005.12.108

1. Introduction

Fukuyama congenital muscular dystrophy (FCMD) is caused by mutations in the fukutin gene (Kobayashi et al., 1998), the product of which is involved in the glycosylation of α-dystroglycan (α-DG) (Aravind and Koonin, 1999; Michele et al., 2002), a central component of the dystrophin–glycoprotein complex (Ervasti and Campbell, 1993; Henry and Campbell, 1999; Ibraghimov-Beskrovnaya et al., 1992). Hypoglycosylation of α-DG results in the decreased binding of laminin at the sarcolemma and in the subsequent dystrophic pathology of skeletal muscles (Michele et al., 2002).

As for the central nervous system, FCMD brains are characterized by cerebral and cerebellar micropolygyria (Kamoshita et al., 1976). Based on the breached glia-limitans and the protrusion of glial–neuronal tissue into the subarachnoid space, a fragile glia-limitans has been hypothesized to be a cardinal feature of the pathological process in FCMD brains (Nakano et al., 1996; Takada et al., 1987). The presence of α-DG in the glia-limitans, and in the glial endfeet of vessel walls (Michele et al., 2002; Zaccaria et al., 2001), supports the hypothesis that hypoglycosylation of α-DG results in decreased binding of glial α-DG with extracellular matrix proteins. Decreased integrity of the glia-limitans may be responsible for the protrusion of brain parenchyma and overmigration of neurons beyond the pial surface during cerebral corticogenesis. However, in contrast to the findings in muscle tissue, hypoglycosylation of α-DG has not been identified in the glia-limitans of FCMD brains. In addition, fukutin protein has been localized in both neurons and glial cells (Ohtsuka-Tsurumi et al., 2004; Saito et al., 2000; Sasaki et al., 2000; Yamamoto et al., 2002). In this study, we immunostained FCMD brains with an antibody that recognizes the polysaccharide epitope of α-DG. Interestingly, the immunoreactivity of glycosylated α-DG in the subpial glia-limitans was not ubiquitously disrupted. On the other hand, hypoglycosylation of α-DG was suggested in hippocampal neurons of FCMD brains. This differential hypoglycosylation may provide a clue to understanding the pathological process in FCMD brains.

2. Results

The α-DG antibody labeled the glia-limitans at the cortical surface and the vessel walls in the control cerebrum (Fig. 1A) and cerebellum (Fig. 1D). In FCMD brains, the continuity of glia-limitans staining was occasionally interrupted at regions with parenchymal protrusions beyond the pial surface (Fig. 1B). Fragmentation of α-DG immunopositive membrane was also noted at the gyral fusion (Fig. 1C). In the FCMD cerebellum, immunostaining at the glia-limitans and vessel walls was comparable to that in the control brains, in areas without micropolygyria (Fig. 1E). The fragmentation of α-DG labeling at the glia-limitans was restricted to the area of micropolygyria (Fig. 1F). Laminin immunolabeling was fragmented and correlated with that of α-DG in the structurally disordered regions of FCMD cerebrum and cerebellum (Figs. 2A and B). α-DG immunolabeling on capillary walls was confirmed by double staining with antifactor VIII (Figs. 2C to E). In the hippocampus, neurons of the dentate gyrus and the corpus ammonis were immunopositive for α-DG in control subjects (Figs. 3A and C), but this staining was markedly decreased in all of the FCMD brains (Figs. 3B and D). In contrast, immunolabeling of blood vessels and the glia-limitans was preserved in this region. The immunolabeling disappeared completely in negative control experiments (not shown). Other than the hippocampus, α-DG immunolabeling was not detected in the cerebral and cerebellar neurons of either control or FCMD brains.

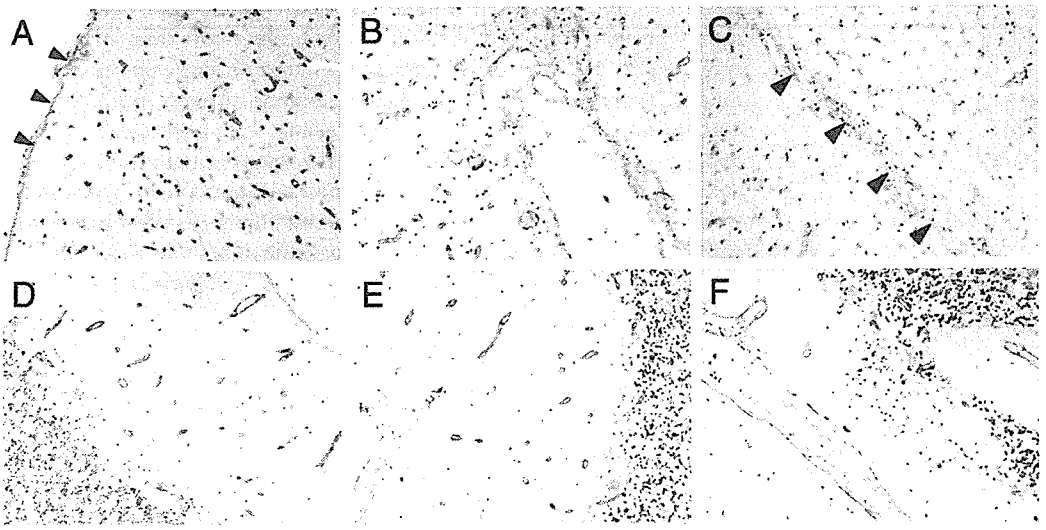

Fig. 1 – α-dystroglycan (α-DG) immunoreactivity in control (A and D) and FCMD (B, C, E, and F) brains. The α-DG positive glia-limitans is continuous in the control cerebrum (arrowheads in A), but fragmentary on the cortical surface (B) and at the cortical fusion (C, arrowheads) in FCMD brains. The continuity of the α-DG positive glia-limitans is preserved in the control cerebellum (D) and in the FCMD cerebellum in areas with normal structure (E), but is disrupted in the FCMD cerebellum in areas of micropolygyria (F). A to F: 200×.

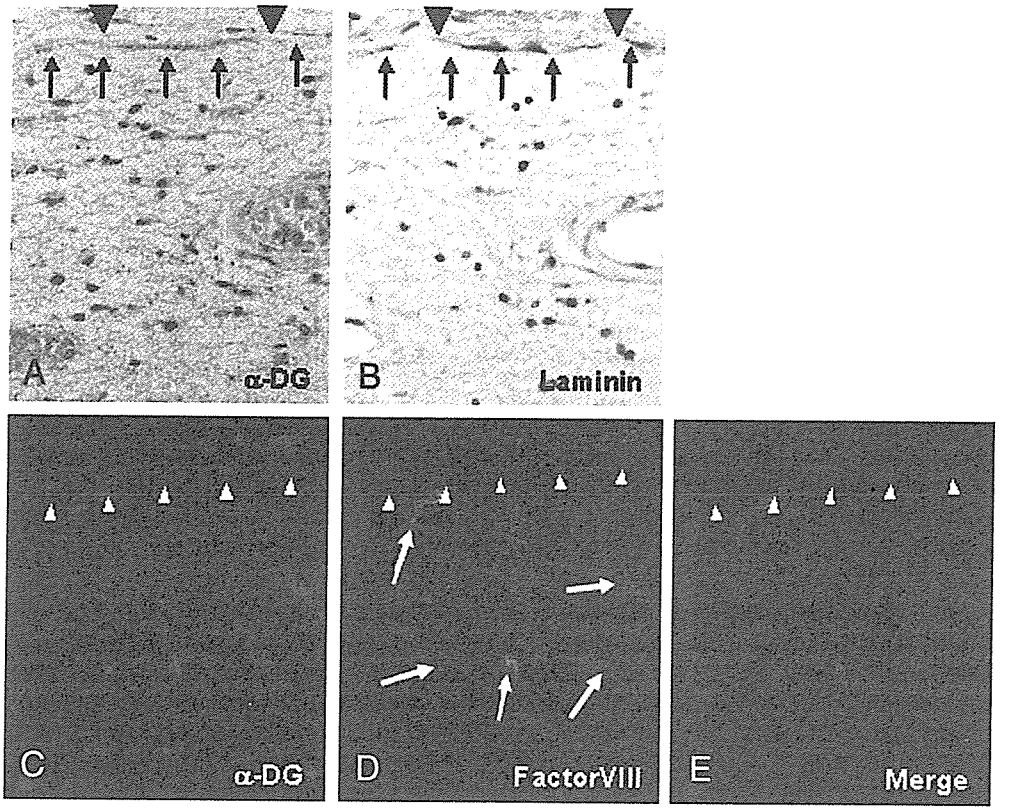

Fig. 2 – (A and B) Immunolabeling of glia-limitans (arrows) with α-DG (A) and laminin (B) is decreased at comparable sites (A and B) in consecutive sections of an FCMD cerebrum. (C–E) α-DG (C) is co-localized with factor VIII (D) at capillary walls. Arrowheads: glia-limitans, arrows: capillaries. A to E: 400×.

The fukutin antisera labeled the neurons of the corpus ammonis (Fig. 4B), and this labeling was decreased in the FCMD brains (Fig. 4C). The labeling of dentate gyrus neurons was weak in control subjects (Fig. 4E) and FCMD patients (Fig. 4F), making the difference between these groups less evident than in the corpus ammonis. Other than this hippocampal expression, immunolabeling was not detected in the cerebral and cerebellar neurons of either control or FCMD brains. No

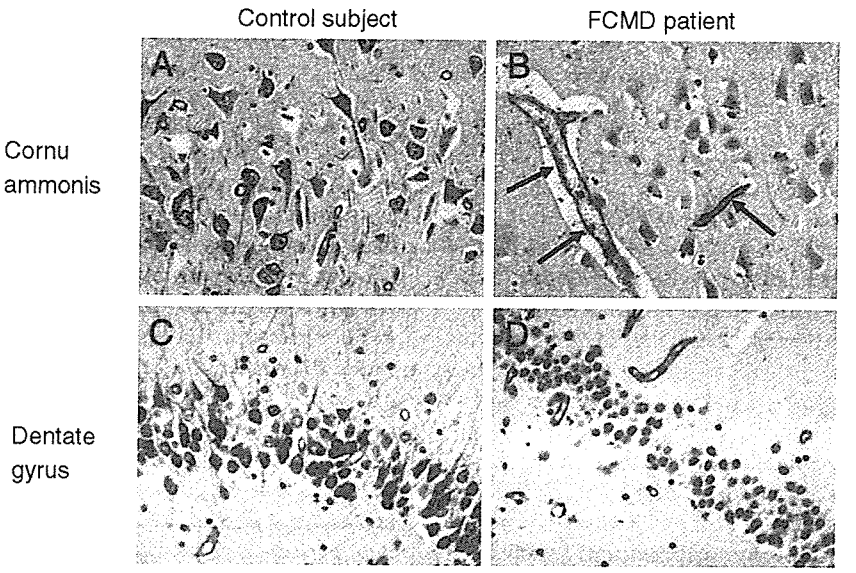

Fig. 3 – α-dystroglycan (α-DG) immunoreactivity in the hippocampus. Neurons in the cornu ammonis 2 area (A) and dentate gyrus (C) are immunopositive for α-DG in control brains, but are immunonegative in FCMD brains (B and D). Note that vessel walls are immunopositive for α-DG in FCMD brains (arrows in panel B). A to D: 400×.

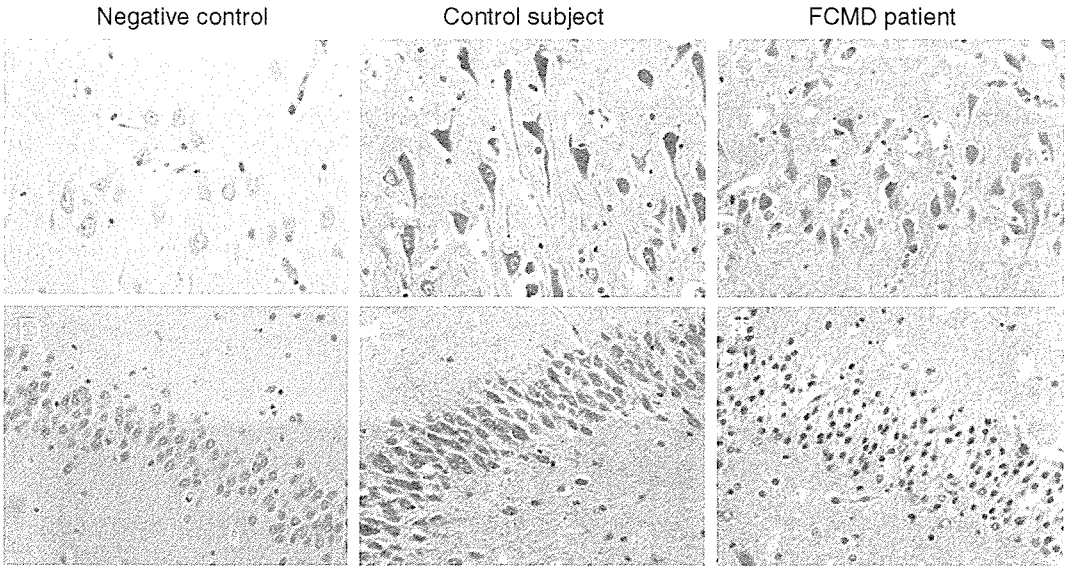

Fig. 4 – Hippocampal fukutin immunoreactivity in control (A, B, D, and E) and FCMD (C and F) brains, stained with the anti-C1 (B, C, E, and F) antiserum. Primary antibody was replaced with preabsorbed antiserum in negative control experiments (A and D). Labeling is intense in neurons of the cornu ammonis in control brains (A), but is diminished in FCMD brains (C). The labeling is weak in the dentate gyrus, and the difference between the control (E) and FCMD (F) is less evident. A to H: 400×.

immunoproducts were seen on slides incubated with the preimmune sera (Figs. 4A and D). The data are summarized in Fig. 5.

3. Discussion

The data presented here suggest co-expression of α-DG and fukutin in the hippocampal neurons of humans. Decreased labeling of α-DG with VIA4-1 in this cell population in FCMD brains supports the involvement of fukutin in the glycosylation process of α-DG, as is the case in skeletal muscle (Hayashi et al., 2001; Michele et al., 2002).

In recent years, α-DG expression in the glia-limitans has been highlighted, since it strongly supports the hypothesis

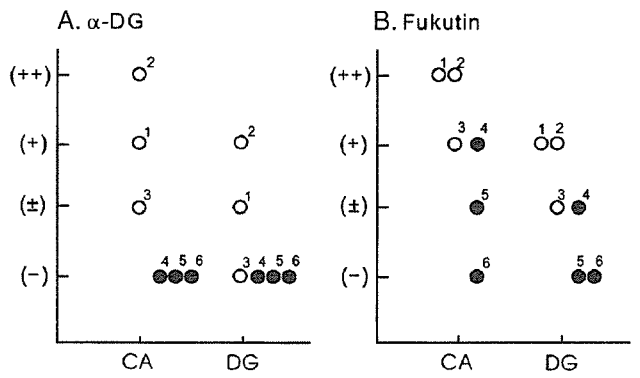

Fig. 5 – Summary of the immunohistochemical findings. Open circle: control subject, filled circle: FCMD patient. (–): negative, (±): weakly positive, (+): moderately positive, (++): intensely positive. CA: cornu ammonis, DG: dentate gyrus. 1 to 3: control subjects, 4 to 6: FCMD patients.

that the fragile glia-limitans is essential to the pathogenesis of micropolygyria. However, there has been controversy regarding the expression pattern of α-DG in the central nervous system. α-DG has been localized to glial cells (Michele et al., 2002; Moore et al., 2002), neurons (Górecki et al., 1994), or both (Zaccaria et al., 2001), in mammalian brains by means of in situ hybridization (Górecki et al., 1994) and immunohistochemistry (Michele et al., 2002; Moore et al., 2002; Zaccaria et al., 2001). Differences in affinity among antibodies may account for this discrepancy, or the antigenicity of α-DG itself may differ between neurons and glial cells, as discussed below. In any case, neuronal expression of α-DG in the hippocampus has been commonly described in several previous reports (Górecki et al., 1994; Zaccaria et al., 2001), and is consistent with the present observations. Decreased immunolabeling of α-DG in hippocampal neurons is compatible with blunted long-term hippocampal potentiation in the brain-selective α-DG knockout mouse (Moore et al., 2002). Since α-DG may participate in synaptic function through clustering of the dystrophin-glycoprotein complex with GABA receptors (Knuesel et al., 2001; Levi et al., 2002; Litov et al., 1990), hypoglycosylation of neuronal α-DG may account for the epileptic seizures and intellectual disabilities of FCMD patients.

Fragmentation of α-DG immunostaining with VIA4-1 antibody correlated with that of laminin immunostaining of glia-limitans at sites of micropolygyria and subarachnoid parenchymal protrusion in FCMD brains. This was compatible with preceding studies using electron microscopy, which showed breaches of the glia-limitans that were penetrated by glial–neuronal tissue (Nakano et al., 1996). On the other hand, unexpectedly, α-DG immunoreactivity with this antibody was preserved in the glia-limitans where the integrity of the cortical structure was preserved, or in the fragmented glia-limitans itself, as well as in vessel walls. This was in

contrast to the reduction of staining in FCMD skeletal muscle with the same antibody (Hayashi et al., 2001). The moiety of the α-DG polysaccharide chain differs between muscle and other tissues. α-DG is identified as a 120-kDa band in brain homogenates, in contrast to the 156-kDa band in skeletal muscle (Campbell and Kahl, 1989; Gee et al., 1993; Herrmann et al., 2000). Hypoglycosylation of α-DG has been identified in FCMD muscles, by demonstrating the absence of monoclonal antibody-reactive α-DG, and the reduction in molecular weight of the core antibody-reactive α-DG (Michele et al., 2002). The former antibodies, including VIA4-1, recognize the polysaccharide epitope, and the latter binds to the polypeptide backbone of α-DG. Hayashi et al. (2001) reported that VIA4-1-reactive α-DG with a normal molecular weight was present but at a reduced level in FCMD brains. Consistent with our present data, they observed the intact staining of blood vessels with this antibody in the FCMD cerebellum. Interestingly, the VIA4-1-reactive punctate labeling of Purkinje cells was reduced in the FCMD brain, in contrast to the normal labeling pattern with a possible core antibody. Taken together, these findings indicate that the α-DG in vascular glial endfeet is normally glycosylated, while the glycosylation of α-DG in neurons is disordered, in FCMD brains. Accordingly, we hypothesize that the glycosylation status of α-DG may differ between neurons and glial cells under physiological conditions. Differential roles of α-DG glycosylation enzymes in individual organs, as identified in the kidney (Grewal et al., 2005), may be extended to this intra-organ differentiation. The VIA4-1 antibody, originally raised against muscle-type α-DG (Ervasti et al., 1990), may have a higher affinity for the polysaccharide epitope of glial cells than for that of neurons. Thus, it is even possible that fukutin and other glycoyslation enzymes (De Bernabé et al., 2002; Grewal et al., 2001; Michele and Campbell, 2003; Yoshida et al., 2001) may have different roles for the glycosylation of neuronal and glial α-DG. This assumption may provide a plausible explanation for the discrepancy between the labeling pattern of the monoclonal and polyclonal α-DG antibodies in brain tissues. Both α-DG and fukutin have been localized to migrating cortical neurons during corticogenesis, but the glycosylation status of α-DG in this population has not been examined in FCMD patients. Further study of this issue is warranted in order to better understand the pathogenesis of morphological and functional abnormalities of FCMD brain.

Although there is a population of immunoreactive α-DG-immunoreactive glial cells in FCMD brain, these cells might be functionally disrupted, via altered glycosylation status and decreased laminin binding affinity. α-DG immunolabeling was further diminished at "breaches" of the glia-limitans, concurrent with loss of laminin immunolabeling. These suggest that laminin binding is disrupted when functional glial α-DG is absent, at sites where the glia-limitans may be particularly fragile. Interestingly, anti-α-DG antibody inhibits migration of cerebellar granule cells, possibly by influencing the attachment of granule neurons to the α-DG-expressing Bergmann glial cells (Qu and Smith, 2004). Disruption of α-DG on glial cells, other than at the glia-limitans, may also be involved in the pathogenesis of micropolygyria in FCMD through a neuronal–glial interaction.

In conclusion, we demonstrated preserved immunolabeling of α-DG polysaccharide chain in glial cells, and a reduction of this labeling in hippocampal neurons, in FCMD brains. Fukutin immunolabeling was also decreased in these neurons. These observations suggest that a fukutin protein defect may result in hypoglycosylation of neurons. The pathogenesis of morphological and functional abnormalities in the FCMD brain should be explored in terms of the functional role of glycosylated α-DG in neurons of developing and mature brains.

4. Experimental procedures

Tissues from three FCMD patients (13–17 years old, M:F = 2:1) and three control subjects (all 14 years of age) were obtained at autopsy. Analysis of the fukutin gene revealed homozygous 3-kb insertions in all three FCMD patients. For immunohistochemistry, we took samples from the cerebral cortex, hippocampus, and cerebellum, and compared the results of FCMD cases with those of control subjects.

Mouse monoclonal antibody against α-DG (VIA4-1; Upstate Biochemistry, Lake Placid, NY, diluted 1:20) was used for immunohistochemistry. VIA4-1 has been shown to recognize the glycosylated epitope of α-DG, and immunolabeling with this antibody is decreased in FCMD muscles (Hayashi et al., 2001). Polyclonal antisera against human fukutin were raised in rabbits as described previously (Saito et al., 2000). Synthetic amino acid peptides, corresponding to residues 37–49 (N1 antigen) and 448–461 (C1 antigen), were used for immunization. The anti-C1 and anti-N1 antisera were diluted at 1:3000 (anti-N1) and 1:2000 (anti-C1) for immunohistochemistry. To identify the structural glia-limitans and capillaries, we performed double staining and immunostaining on consecutive sections using antibodies to α-DG and laminin (rabbit polyclonal, 1:20, Progen, Heidelberg) or factor VIII (rabbit polyclonal, 1:50, ZYMED, South San Francisco, CA). For negative control experiments, the primary antisera were omitted or replaced with preimmune sera of rabbits (for fukutin).

After deparaffinization, the sections were immersed in 3% hydrogen peroxide in phosphate-buffered saline (PBS) for 5 min to abolish endogenous peroxidase activity. Microwave treatment for 13 min at 95 °C was performed to retrieve the antigens. Nonspecific binding was blocked with 10% horse serum. The sections were then incubated for 48 h at 4 °C with the primary antibody, followed by incubation with biotinylated goat anti-mouse IgG antibody for 1 h and then with preoxidase-conjugated streptavidin–biotin complex (Vecstatin ABC kit, Vector, Burlingame, CA) at room temperature for 30 min. Between steps, the sections were washed thoroughly three times in PBS. The immunoproducts were visualized with 0.05% 3,3′-diaminobenzidine and 0.0085% H_2O_2 in PBS. The specimens were counterstained with hematoxylin. For double staining, Cy3-conjugated anti-rabbit IgG (1:200, Jackson Immunoresearch Laboratory, West Grove, PA) and FITC-conjugated donkey anti-mouse IgG (1:200, Jackson Immunoresearch Laboratory) were used as secondary antibodies and were incubated for 6 h.

REFERENCES

Aravind, L., Koonin, E.V., 1999. The fukutin protein family-predicted enzymes modifying cell-surface molecules. Curr. Biol. 9, R836–R837.

Campbell, K.P., Kahl, S.D., 1989. Association of dystrophin and an integral membrane protein. Nature 338, 259–262.

De Bernabé, D.B.-V., Currier, S., Steinbrecher, A., Celli, J., van Beusekom, E., van der Zwaag, B., Kayserili, H., Merlini, L., Chitayat, D., Dobyns, W.B., Cormand, B., Lehesjoki, A.-E., Cruces, J., Voit, T., Walsh, C.A., van Bokhoven, H., Brunner, H.G., 2002. Mutations in the O-mannosyltransferase gene *POMT1* give rise to the severe neuronal migration disorder Walker–Warburg syndrome. Am. J. Hum. Genet. 71, 1033–1043.

Ervasti, J.M., Campbell, K.P., 1993. A role for the dystrophin–glycoprotein complex as a transmembrane linker between laminin and actin. J. Cell Biol. 122, 809–823.

Ervasti, J.M., Ohlendieck, K., Kahl, S.D., Gaver, M.G., Campbell, K.P., 1990. Deficiency of a glycoprotein component of the dystrophin complex in dystrophic muscle. Nature 345, 315–319.

Gee, S.H., Blacher, R.W., Douville, P.J., Provost, P.R., Yurchenco, P.D., Carbonetto, S., 1993. Laminin-binding protein 120 from brain is closely related to the dystrophin-associated glycoprotein, dystroglycan, and binds with high affinity to the major heparin binding domain of laminin. J. Biol. Chem. 268, 14972–14980.

Górecki, D.C., Derry, J.M.J., Barnard, E.A., 1994. Dystroglycan: brain localization and chromosome mapping in the mouse. Hum. Mol. Genet. 3, 1589–1597.

Grewal, P.K., Holzfeind, P.J., Bittner, R., Hewitt, J.E., 2001. Mutant glycosyltransferase and altered glycosylation of α-dystroglycan in the myodystrophy mouse. Nat. Genet. 28, 151–154.

Grewal, P.K., McLaughlan, J.M., Moore, J.C., Browning, C.A., Hewitt, J.E., 2005 (Jun 15). Characterization of the LARGE family of putative glycosyltransferases associated with dystroglycanopathies. Glycobiology 15, 912–923.

Hayashi, Y.K., Ogawa, M., Tagawa, K., Noguchi, S., Ishihara, T., Nonaka, I., Arahata, K., 2001. Selective deficiency of α-dystroglycan in Fukuyama-type congenital muscular dystrophy. Neurology 57, 115–121.

Henry, M.D., Campbell, K.P., 1999. Dystroglycan inside and out. Curr. Opin. Cell Biol. 11, 602–607.

Herrmann, R., Straub, V., Blank, M., Kutzick, C., Franke, N., Jacob, E.N., Lenard, H.G., Kröger, S., Voit, T., 2000. Dissociation of the dystroglycan complex in caveolin-3-deficient limb girdle muscular dystrophy. Hum. Mol. Genet. 9, 2335–2340.

Ibraghimov-Beskrovnaya, O., Ervasti, J.M., Leveille, J., Slaughter, C.A., Sernett, S.W., Campbell, K.P., 1992. Primary structure of dystrophin-associated glycoproteins linking dystrophin to the extracellular matrix. Nature 355, 696–702.

Kamoshita, S., Konishi, Y., Segawa, M., Fukuyama, Y., 1976. Congenital muscular dystrophy as a disease of the central nervous system. Arch. Neurol. 33, 513–516.

Knuesel, I., Zuellig, R.A., Schaub, M.C., Fritschy, J.-M., 2001. Alterations in dystrophin and utrophin expression parallel the reorganization of GABAergic synapses in a mouse model of temporal lobe epilepsy. Eur. J. Neurosci. 13, 1113–1124.

Kobayashi, K., Nakahori, Y., Miyake, M., Matsumura, K., Kondo-Iida, E., Nomura, Y., Segawa, M., Yoshioka, M., Saito, K., Osawa, M., Hamano, K., Sakakihara, Y., Nonaka, I., Nakagome, Y., Kanazawa, I., Nakamura, Y., Tokunaga, K., Toda, T., 1998. An ancient retrotransposal insertion causes Fukuyama-type congenital muscular dystrophy. Nature 394, 388–392.

Levi, S., Grady, R.M., Henry, M.D., Campbell, K.P., Sanes, J.R., Craig, A.M., 2002. Dystroglycan is selectively associated with inhibitory GABAergic synapses but is dispensable for their differentiation. J. Neurosci. 22, 4274–4285.

Litov, H.G.W., Byers, T.J., Watkins, S.C., Kunkel, L.M., 1990. Localization of dystrophin to postsynaptic regions of central nervous system cortical neurons. Nature 348, 725–728.

Michele, D.E., Campbell, K.P., 2003. Dystrophin-glycoprotein complex: post-translational processing and dystroglycan function. J. Biol. Chem. 278, 15457–15460.

Michele, D.E., Barresi, R., Kanagawa, M., Saito, F., Cohn, R.D., Satz, J.S., Dollar, J., Nishino, I., Kelley, R.I., Somer, H., Straub, V., Mathews, K.D., Moore, S.A., Campbell, K.P., 2002. Post-transcriptional disruption of dystroglycan–ligand interactions in congenital muscular dystrophies. Nature 418, 417–422.

Moore, S.A., Saito, F., Chen, J., Michele, D.E., Henry, M.D., Messing, A., Cohn, R.D., Ross-Barta, S.E., Westra, S., Williamson, R.A., Hoshi, T., Campbell, K.P., 2002. Deletion of brain dystroglycan recapitulates aspects of congenital muscular dystrophy. Nature 418, 422–425.

Nakano, I., Funahashi, M., Takada, K., Toda, T., 1996. Are breaches in the glia limitans the primary cause of the micropolygyria in Fukuyama-type congenital muscular dystrophy (FCMD)? Pathological study of the cerebral cortex of an FCMD fetus. Acta Neuropathol. 91, 313–321.

Ohtsuka-Tsurumi, E., Saito, Y., Yamamoto, T., Voit, T., Kobayashi, M., Osawa, M., 2004. Co-localization of fukutin and alpha-dystroglycan in the mouse central nervous system. Brain Res. Dev. Brain Res. 152, 121–127.

Qu, Q., Smith, F.I., 2004. Alpha-dystroglycan interactions affect cerebellar granule neuron migration. J. Neurosci. Res. 76, 771–782.

Saito, Y., Mizuguchi, M., Oka, A., Takashima, S., 2000. Fukutiin protein is expressed in neurons of the normal developing human brain but is reduced in Fukuyama-type congenital muscular dystrophy brain. Ann. Neurol. 47, 756–764.

Sasaki, J., Ishikawa, K., Kobayashi, K., Kondo-Iida, E., Fukayama, M., Mizusawa, H., Takashima, S., Sakakihara, Y., Nakamura, Y., Toda, T., 2000. Neuronal expression of the fukutin gene. Hum. Mol. Genet. 9, 3083–3090.

Takada, K., Nakamura, H., Suzumori, K., Ishikawa, T., Sugiyama, N., 1987. Cortical dysplasia in a 23-week fetus with Fukuyama congenital muscular dystrophy (FCMD). Acta Neuropathol. 74, 300–306.

Yamamoto, T., Kato, Y., Karita, M., Takeiri, H., Muramatsu, F., Kobayashi, M., Saito, K., Osawa, M., 2002. Fukutin expression in glial cells and neurons: implication in the brain lesions of Fukuyama congenital muscular dystrophy. Acta Neuropathol. 104, 217–224.

Yoshida, A., Kobayashi, K., Manya, H., Taniguchi, K., Kano, H., Mizuno, M., Inazu, T., Mitsuhashi, H., Takahashi, S., Takeuchi, M., Herrmann, R., Straub, V., Talim, B., Voit, T., Topaloglu, H., Toda, T., Endo, T., 2001. Muscular dystrophy and neuronal migration disorder caused by mutations in a glycosyltransferase, POMGnT1. Dev. Cell 1, 717–724.

Zaccaria, M.L., Di Tommaso, F., Brancaccio, A., Paggi, P., Petrucci, T.C., 2001. Dystroglycan distribution in adult mouse brain: a light and electron microscopy study. Neuroscience 104, 311–324.

Epilepsia, 47(6):991–997, 2006
Blackwell Publishing, Inc.

Magnetoencephalography in Patients with Tuberous Sclerosis and Localization-related Epilepsy

*†Takanori Kamimura, †Jun Tohyama, ‡Makoto Oishi, †Noriyuki Akasaka, †Osamu Kanazawa, §Mutsuo Sasagawa, ||Mitsuhiro Kato, ¶Kousaku Ohno, ‡Hiroshi Masuda, ‡Shigeki Kameyama, and *Makoto Uchiyama

**Division of Pediatrics, Department of Homeostatic Regulation and Development, Course for Biological Functions and Medical Control, Niigata Graduate School of Medical and Dental Sciences, and Departments of †Pediatric Neurology, ‡Neurosurgery, and §Psychiatry, Epilepsy Center, Nishi-Niigata Chuo National Hospital, Niigata; ||Department of Pediatrics, Yamagata University School of Medicine, Yamagata; and ¶Division of Child Neurology, Institute of Neurological Sciences, Faculty of Medicine, Tottori University, Yonago, Japan*

Summary: *Purpose:* To clarify the usefulness of magnetoencephalography (MEG) for diagnosis of the spatial relations between spike foci and suspicious epileptogenic tubers on MRI in patients with tuberous sclerosis (TS) and to compare MEG spike foci with single-photon emission computed tomography (SPECT) findings.

Methods: We analyzed magnetic fields of epileptic spike discharges in 15 patients with TS and localization-related epilepsy (LRE) by using MEG (a whole-head 204-channel magnetometer system). We investigated the spatial relation between the equivalent current dipoles (ECDs) of interictal spike discharges and visible cortical tubers on MRI. We also compared results of MEG and MRI with SPECT findings.

Results: MEG detected a cluster of ECDs around one cortical tuber in six of 15 patients and clusters of ECDs around two cortical tubers in five patients. Interictal SPECT was disappointing in detection of epileptic foci in TS. However, MEG spike foci showed spatial consistency with ictal hyperperfusion areas in two patients. Three patients with single ECD clusters underwent surgical treatment: two have been seizure free, and one has obtained seizure reduction of >90%.

Conclusions: ECDs were located around visible tuber nodules. MEG enabled precise localization of the epileptic foci and provided crucial information for surgical treatment in patients with TS and partial epilepsy. TS patients showing a single ECD cluster on MEG may be appropriate candidates for surgical treatment. **Key Words**: Tuberous sclerosis—Symptomatic localization-related epilepsy—Magnetoencephalography—SPECT—Epileptic focus.

Tuberous sclerosis (TS) is a multisystem disorder of tissue growth and differentiation characterized by tumors in the brain, eyes, heart, and kidneys, and by cutaneous abnormalities (1,2). TS is inherited as an autosomal dominant trait with high penetrance and variable expressivity. However, about two thirds of TS cases are sporadic, resulting from spontaneous genetic mutations in the offspring of healthy parents (1,3). Mutations or deletions of two separate genes, *TSC1* and *TCS2*, have been identified in patients with TS (3).

One of the most important complications of TS is epilepsy. Infantile spasms are the most common type of seizure at presentation (4). Partial seizures are often seen, whereas generalized seizures are relatively rare (1,4). Epileptic foci are generally restricted to a limited cortical area, even when multiple cortical tubers are present (5,6). Several authors reported that surgical treatment of patients with TS and intractable epilepsy is most effective if a single tuber or true epileptic foci can be identified as the source of seizures and resected. (5–8). In the presence of multiple cortical tubers, preoperative evaluation with multiple modalities such as scalp video-EEG monitoring, positron emission tomography, single-photon emission computed tomography (SPECT), and magnetoencephalography (MEG) is considered necessary for the accurate identification of true epileptic foci. However, only a few reports on evaluation of MEG in TS patients have been published (9,10). These studies did not use a whole-head magnetometer for evaluating ECDs, and no MEG studies have been preformed with a large number of TS patients. The aims of the present study were to clarify the usefulness of the whole-head MEG system in determining the spatial relation between the MEG spike

Accepted November 30, 2005.
Address correspondence and reprint requests to Dr. J. Tohyama at Department of Pediatric Neurology, Epilepsy Center, Nishi-Niigata Chuo National Hospital, Masago 1-14-1, Niigata 950-2085, Japan. E-mail: jtohyama@masa.go.jp

foci and suggestive epileptogenic tubers on MRI and to compare MEG spike foci with SPECT findings for the diagnosis of epileptic foci in patients with TS.

METHODS

Patients

From all patients who attended the Epilepsy Center, Nishi-Niigata Chuo National Hospital between January 2000 and March 2005, 15 patients diagnosed with both TS and localization-related epilepsy (LRE) (seven male and eight female patients, age 2–40 years; mean, 15.1 years) were selected (Table 1). TS was diagnosed on the basis of skin lesions and multiple cortical tubers on MRI that exhibited calcification on computed tomography (CT), whereas symptomatic LRE (SLRE) was diagnosed according to criteria of the International Classification of Epilepsies and Epileptic Syndromes (11). In two patients (cases 2 and 13), mutations of *TSC1* and *TSC2* were investigated with polymerase chain reaction (PCR)-single-strand conformational polymorphism (SSCP) and sequencing analysis by using DNA from peripheral leukocytes, confirming the clinical diagnosis. A missense mutation of 4952A>G (N1651S) was found in *TSC2* in case 2, and a nonsense mutation of 3355C>G (Q1119X) was found in *TSC2* in case 13; both mutations were heterozygous. All patients experienced complex partial seizures (CPSs); one patient (case 3) also had secondarily generalized tonic–clonic seizures. Five patients had daily seizures (cases 1, 2, 7, 10, and 14), six had weekly seizures (cases 3, 4, 5, 6, 11, and 12), and four had monthly seizures (cases 8, 9, 13, and 15). Five patients had a history of West syndrome (cases 1, 4, 8, 11, and 13), and three of these five patients had received adrenocorticotropic hormone (ACTH) therapy (cases 4, 11 and 13). All patients had intractable seizures, and various antiepileptic drugs (AEDs) were administered for treatment (Table 1). Tailored-focus resection was performed in three patients (cases 2, 4, and 7).

All 15 patients underwent MRI, MEG, and interictal SPECT. Cases 1, 2, 8, and 13 were sedated because they were too young to cooperate with examinations. The remaining patients remained conscious during examinations. In two cases (cases 2 and 7), ictal SPECT was successfully obtained in addition to interictal SPECT. We also compared localization of the ictal hyperperfusion area with the MEG spike foci.

MRI

To detect epileptogenic lesions, T_1-weighted (T_1-W), T_2-weighted, proton-density weighted (PDW), and fluid-attenuated inversion recovery (FLAIR) MR images were routinely taken with a 1.5-Tesla system (MAGNEX Epios15; Shimadzu, Kyoto, Japan). Both PDW and FLAIR MR were more sensitive for determining the precise location and extent of cortical tubers in each TS patient. We compared localization of cortical tubers on PDW and FLAIR MR images with clusters of ECDs demonstrated by MEG on T_1-W MR images.

MEG

MEG was performed with a whole-scalp neuromagnetometer (Neuromag 204; Elekta-Neuromag, Oy, Finland) in a magnetically shielded room. This device uses 204 planar-type, first-order gradiometers. Before recording, for data reference, we digitized the positions of three anthropometric points (nasion and bilateral preauricular points) and four indicator coils on the scalp with a three-dimensional electromagnetic digitizer (Polhemus, Colchester, VT, U.S.A.). MEG recordings were analyzed with a band-pass filter between 3 and 45 Hz. We analyzed the amplitude of MEG spikes at the MEG sensor location with the highest amplitude. For each MEG spike, we calculated the single ECD source at the initial spike peak with a spherical model. ECD spike sources with goodness-of-fit (GOF) >80% were accepted as valid. Of 204 MEG sensors, we used data from 40 neighboring sensors that encompassed both extremes of the magnetic flux distribution associated with each event. We evaluated dipole moments of the MEG spike sources and overlaid the spike sources onto T_1-W MR images of the patient's head with respect to the three morphometric points. MRI was performed with a 1.5-Tesla system, as described earlier.

SPECT

After the intravenous injection of 600 mBq of ^{99m}Tc-ethyl cysteinate dimer (^{99m}Tc-ECD) for adults, or 600 $\times$ (body weight/60)$^{2/3}$ mBq of ^{99m}Tc-ECD for children, SPECT imaging was performed with a PRISM 2000XP (Shimadzu, Kyoto, Japan). A series of 12-mm contiguous slices perpendicular to the orbitomeatal line were obtained for each patient. Ictal scans were obtained by promptly injecting the tracer through a preplaced venous line at the onset of electroclinical seizure detected by continuous video-EEG recording. In one patient, an ictal scan was evaluated by using three-dimensional stereotactic surface projections (3D-SSP) (12) and subtraction ictal SPECT coregistered to MRI (SISCOM) (13) as described.

Surgical treatment

After therapeutic evaluation, three of the 15 patients underwent surgical treatment. As part of the preoperative evaluation, long-term electrocorticography (ECoG) was performed to localize the seizure focus precisely in cases 4 and 7; this was facilitated by implantation of subdural electrodes according to MEG and SPECT results. Case 2 was too young for the implantation of subdural electrodes to be attempted. Localization of resection was decided according to the results of scalp video-EEG, MEG, ictal SPECT, and intraoperative ECoG. All patients underwent tailored-focus resection in addition to tuberectomy.

TABLE 1. *Clinical characteristics and results of investigations for fifteen study patients*

Patient	Sex	Age (yr)	Epilepsy type	Type of seizure	Seizure frequency	Major tubers on MRI	ECDs on MEG	Hypoperfusion on interictal SPECT	Hyperperfusion on ictal SPECT	AED
1	F	2	WS→LRE	CPS	Daily	Lt Fr	Lt Fr	None	n.d.	VPA, CLB, ZNS, PHT, PRM, CZP, SLT, CBZ, KBr, ACZ
2	M	2	LRE	CPS→sGTC	Daily	Lt Fr[a], Lt O[a]	Lt P	Lt Fr,P	Lt P	PHT, VPA, PRM, CBZ, ZNS, CZP, PB
3	M	15	LRE	CPS	Weekly	Rt F	Rt T	Bil Fr,P	n.d.	VPA, CBZ, CZP, PHT
4	M	24	WS→LRE	CPS	Weekly	Rt Fr[a], Lt Fr	Rt Fr	Bil Fr	n.d.	CBZ, ZNS, VPA, PHT, CZP, CLB
5	F	25	LRE	CPS	Weekly	Lt F, Rt P	Lt Fr	M-hypo	n.d.	VPA, PHT, PB, CBZ, PRM, ZNS, CZP
6	M	28	LRE	CPS	Weekly	Rt P, Rt O	Lt O	Rt P	n.d.	VPA, PHT, CBZ
7	M	24	LRE	CPS	Daily	Rt Fr[a]	Rt Fr	M-hypo	Rt Fr[b]	VPA, PHT, CBZ, ZNS, CLB
8	M	4	WS→LRE	CPS	Monthly	Lt Fr, Lt P[a], Rt T, Rt P	Rt Fr, Rt T, Rt P, Rt O	None	n.d.	CZP, ZNS, VPA, PHT, CBZ, CLB
9	F	13	LRE	CPS	Monthly	Lt Fr, Lt P	Lt P, Rt O	M-hypo	n.d.	VPA, ZNS, CBZ, CZP
10	F	15	LRE	CPS	Daily	Lt Fr, Rt Fr, Rt P	Lt Fr, Rt Fr, Rt P	Rt Fr,T,Lt T	n.d.	PB, VPA, CBZ, PHT, ACZ, ESM, ZNS, SLT, NZP
11	M	21	WS→LRE	CPS	Weekly	Rt Fr, Rt O	Lt O, Rt Fr	M-hypo	n.d.	DZP, VPA, NZP, PB, CLB, PRM, CZP, CBZ, PHT
12	F	40	LRE	CPS	Weekly	Lt Fr, Lt P, Rt Fr, Rt P	Rt P, Rt T	Bil Fr,P, Rt O,P	n.d.	CZP, PHT, PB, CLB
13	F	2	WS→LRE	CPS	Monthly	Lt Fr, Rt Fr, Rt T, Rt P	None	Bil Fr,P	n.d.	NZP, CBZ, VPA, ZNS, PHT, CLB, CBZ, KBr
14	F	16	LRE	CPS	Daily	Rt Fr, Rt P	None	None	n.d.	VPA, ESM, ZNS, CZP, PHT, CBZ, APT
15	F	13	LRE	CPS	Monthly	Lt Fr, Lt T, Rt F	None	Rt Fr	n.d.	CBZ, ZNS, CZP, CLB
	Mean,	16.3								

F, female; M, male; WS, West syndrome; LRE, localization-related epilepsy; CPS, complex partial seizure; sGTC, secondarily generalized tonic–clonic convulsion; Lt, left; Rt, right; Bil, bilateral; Fr, frontal; P, parietal; T, temporal; O, occipital; M-hypo, multiple hypoperfusion areas; n.d., not done; None, no detectable findings; AED, antiepileptic drug; APT, acetylpheneturide; ACZ, acetazolamide; CBZ, carbamazepine; CLB, clobazam; CZP, clonazepam; DZP, diazepam; ESM, ethosuximide; KBr, potassium bromide; NZP, nitrazepam; PB, phenobarbital; PHT, phenytoin; PRM, primidone; SLT, sulthiame; VPA, valproate acid; ZNS, zonisamide.

[a]Calcified tuber.

[b]Findings on 3D-SSP and SISCOM.

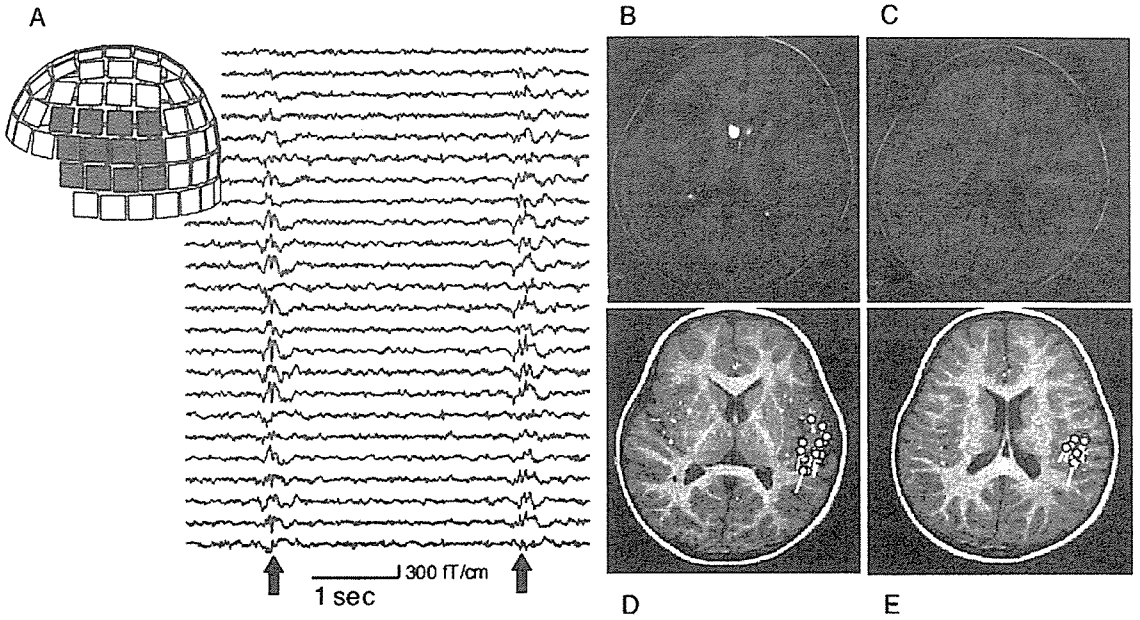

FIG. 1. Raw interictal magnetoencephalography (MEG) data recorded from 24 sensors covering the left temporal area, fluid-attenuated inversion recovery (FLAIR) magnetic resonance imaging (MRI) and an equivalent current dipole (ECD) cluster from spike discharges on MEG: Case 1. **A:** Raw interictal MEG data: MEG spikes were clearly identified from sensors covering the left temporal area (*arrows*). **B, C:** FLAIR MRI shows multiple high-intensity areas. **D, E:** An ECD cluster from spike discharges on MEG (white) are superimposed on T_1-weighted MRI. ECDs are located adjacent to and surrounding the cortical tubers in the left frontal and temporal lobes.

RESULTS

Table 1 summarizes the clinical data and results of investigations.

MRI

PDW and FLAIR MRI clearly demonstrated cortical tubers as hyperintense areas in all TS patients (Figs. 1B and C, 2A, and 3A). On the whole, cortical tubers were diffusely disseminated throughout the cerebral cortices or around the lateral ventricles. In 11 of 15 patients (cases 1–4, 8–14), multiple (more than five) cortical tubers were detected. The remaining patients (cases 5–7, 15) had two or three tubers.

MEG

In six (40.0%) of 15 patients (cases 1–5, 7), ECDs were clustered in the area adjacent to and surrounding one specific cortical tuber, suggesting that this was the epileptic focus (Figs. 1 A, D, and E, 2B, and 3B). In five (33.3%) of 15 patients (cases 8–12), ECDs were localized to areas surrounding two or three independent cortical tubers. In one (6.7%) patient, ECDs were clustered in an area where no definite cortical tuber was seen on PDW and FLAIR MRI (case 6). In three (20%) of 15 patients, no ECD clusters were detected (cases 13–15). Other than the fact that ECDs were generally located around tubers, the orientations of ECD clusters were random.

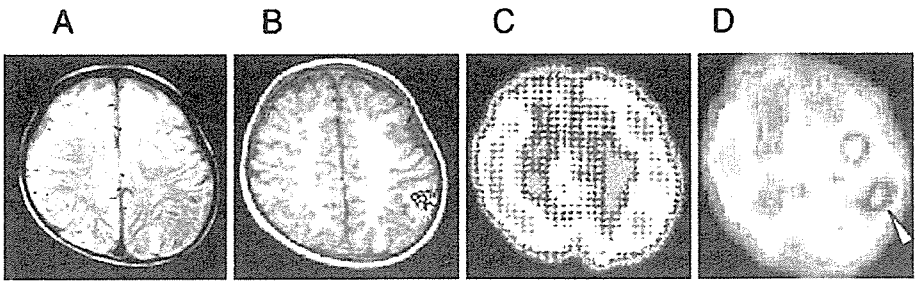

FIG. 2. Magnetic resonance imaging (MRI), magnetoencephalography (MEG), and single-photon emission computed tomography (SPECT) findings: Case 2. **A:** Proton density-weighted MRI reveals diffuse multiple high-intensity areas, indicating cortical tubers. **B:** MEG: An equivalent current dipole (ECD) cluster (yellow), superimposed on T_1-weighted MRI, is detected in the left parietal lobe. **C:** Interictal SPECT: Hypoperfusion areas are shown in the right frontal and the left parietal lobes. **D:** Ictal SPECT: A hyperperfusion area (*white arrowhead*) is seen in the left parietal area. It is spatially consistent with an ECD cluster on MEG. Another hyperperfusion area is regarded as secondary hyperperfusion because of cortical tubers.

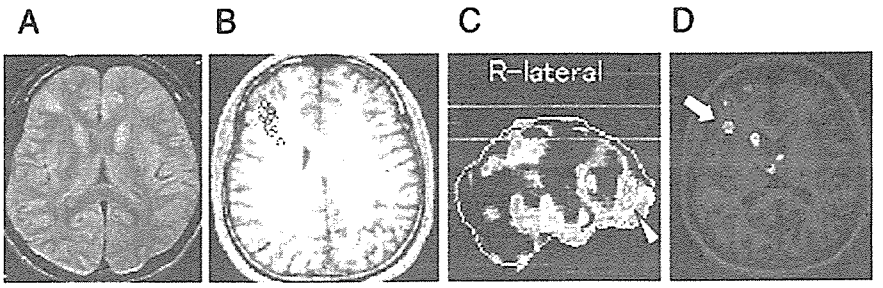

FIG. 3. Magnetic resonance imaging (MRI), magnetoencephalography (MEG), and single-photon emission computed tomography (SPECT) findings: Case 7. **A:** Proton density-weighted MRI: High-intensity areas are seen in the right frontotemporal and the left frontal lobes. **B:** MEG: An equivalent current dipole (ECD) cluster (yellow) is detected adjacent to and surrounding a single tuber in the right frontal lobe. **C, D:** Ictal SPECT: On simple ictal SPECT, no hyperperfusion area is recognized (data not shown). However, after processing of original images by using 3D-SSP **(C)** or SISCOM **(D)** technology, a hyperperfusion area, indicated by a *white arrowhead* **(C)** and a *white arrow* **(D)**, emerged in the right frontal lobe. These images are spatially consistent with the location of an ECD cluster on MEG.

SPECT

In interictal SPECT, multiple hypoperfusion areas consistent with cortical tubers on MRI were apparent in 10 (66.7%) of 15 patients (cases 2–5, 7, 9–13) (Fig. 2C). A single hypoperfusion area was detected in two (13.3%) patients (cases 6 and 15). No hypoperfusion areas were found in three (20.0%) patients (cases 1, 8, and 14).

Although interictal abnormal SPECT findings were not consistent with MEG spike foci in all 15 patients, ictal SPECT obtained from cases 2 and 7 showed hyperperfusion areas consistent with MEG spike foci (Figs. 2D, and 3C and D).

Surgery

After preoperative evaluation, surgery was performed in three patients (cases 2, 4, and 7), all of whom exhibited a single ECD cluster on MEG. In case 2, localization of ECDs was consistent with the hyperperfusion area on ictal SPECT, and this region was resected. Although seizures recurred immediately after the operation, appropriate AEDs eventually eliminated seizures. In case 4, although ictal SPECT was unsuccessful, MEG findings were spatially consistent with the onset zone of seizures on ictal electrocorticography (ECoG). Seizures disappeared postoperatively in this case. Patient 7 underwent surgical resection according to the findings of MEG, ECoG, SISCOM, and 3D-SSP. No seizures have occurred postoperatively. Over a mean follow-up period of 36 months, cases 4 and 7 were assessed as seizure free, and case 2 also achieved >90% seizure reduction. Postoperative MEG showed no residual spike discharge in cases 4 and 7; however, residual ECDs were confirmed around the resected region in case 2. After surgery, higher brain functions were measured by WAIS-R (case 7) or Suzuki-Binet (case 4) in cases 4 and 7 when compared with that measured preoperatively. Patient 2 was too young to undergo evaluation of cognitive function. However, in this patient, development progressed gradually, and surgical intervention prevented deterioration: his developmental quotient remained very similar preoperatively and 3 years postoperatively. In all three patients, AEDs requirements were reduced postoperatively.

DISCUSSION

We investigated the localization of ECDs on MEG in 15 patients with concurrent TS and LRE. Of 15 patients, six (40.0%) exhibited a single ECD cluster around a single tuber, whereas five (33.3%) demonstrated ECDs around two or more tubers. On MRI, 11 patients showed multiple (more than five) cortical tubers, and the remaining patients had two or three tubers, confirming the findings observed in previous reports of TS (14). Although multiple tubers were present, ECDs were detected only adjacent to and surrounding epileptogenic tubers. The present MEG findings implied that a single epileptic focus might have been present in several of the TS patients, even though multiple tubers were observed on MRI. In three cases in our series, localized ECDs were not detected. Previously, only two authors described MEG findings in small numbers of TS patients evaluated with limited sensor arrays (9,10). We reported MEG findings in TS for a large number of patients evaluated with whole-head MEG systems. As TS is characterized by multiple lesions throughout the brain, we consider a whole-head MEG system to be appropriate for evaluating such patients. With such an apparatus, we successfully revealed ECDs located adjacent to and surrounding specific tubers among multiple brain lesions in TS. ECDs were located in an area where no cortical tubers were observed on PDW and FLAIR MRI in only one patient. MRI is not yet sophisticated enough to depict all the cortical tubers that can be identified by gross inspection of the sectioned brain (15,16). Moreover, the correlation between MRI and EEG findings is not absolute (16). It is accordingly possible that latent cortical tubers that are not detected by MRI may have strong epileptogenic activity.

Surgical indications and procedures for patients with TS and epileptic seizures are still controversial. Some authors stress the difficulty of surgical treatments for TS patients with multiple tubers and LRE (17). No crucial

criteria exist for selecting surgical candidates in this patient group. We performed both focus resection and tuberectomy in three patients with a single ECD cluster on MEG and found MEG findings to be useful in determining the specific tuber directly related to the epileptic focus. In the present series, two patients achieved a seizure-free outcome, whereas seizure frequency decreased and AEDs could be reduced in another. Postoperative MEG indicated that all epileptogenic regions had been resected in two patients; however, residual seizures might relate to the residual ECDs around the resected region in case 2. Our findings strongly suggest that ECD clusters are well correlated with epileptogenic zones and that TS patients with medically refractory LRE who exhibit a single ECD cluster on MEG may be appropriate candidates for surgical treatment. However, isolated lesionectomy based on MRI findings alone might be insufficient to control future seizure foci (18).

Focal cortical dysplasia (FCD) is an organic lesion characterized by an epileptogenic cerebral cortical nodule. Several authors have reported MEG findings for patients with FCD, indicating that ECDs of spike discharges were located in the actual FCD nodules (19–21). However, in 11 of our series of 15, ECDs were located in the vicinity of tuberous nodules, a finding in accordance with previous reports (9,10). A recent study using molecular biologic techniques described the relation between FCD of Taylor's balloon cell type and mutation of the *TSC1* gene (22). FCD is well known to have intrinsic epileptogenicity. Our results, however, suggest that the epileptic focus in TS is not anticipated to be within lesions visible on MRI, as is the case in dysembryoplastic neuroepithelial tumor (23). Hence it cannot be assumed that tuberectomy is an ideal surgical strategy for epilepsy patients with TS.

On interictal SPECT, most tubers were recognized as hypoperfusion areas. In SLRE, epileptogenic areas often demonstrate hyperperfusion in the ictal phase and hypoperfusion in the interictal period (24,25). It is difficult to identify epileptogenic areas by interictal SPECT in TS, as multiple tubers give rise to many hypoperfusion areas. We therefore consider MEG to be far superior to interictal SPECT in identifying true epileptic foci in patients with TS. Conversely, Koh (6) reported that ictal SPECT revealed hyperperfusion areas corresponding to epileptogenic lesions in 10 of 21 patients with TS and LRE. We also confirmed ictal hyperperfusion areas consistent with localization of ECDs on MEG in two cases. Although ictal SPECT findings are considered reliable in determining epileptogenic regions, unfortunately epileptic seizures are usually unpredictable. It is therefore not feasible to perform ictal SPECT in every case. Our findings indicate that despite the recording of interictal phenomena, MEG is as useful as ictal SPECT for identifying epileptic foci in patients with TS.

In conclusion, whole-head MEG revealed ECD clusters adjacent to and surrounding epileptogenic tubers. This suggests that epileptic foci are located in the extrinsic area surrounding the tubers. Hence our study provides support for the role of MEG in enabling precise identification of true epileptic foci and providing crucial information for surgical planning in patients with TS and intractable epilepsy. It should be emphasized that TS patients with a single ECD cluster on MEG may be appropriate candidates for surgical treatment. The present study also suggests that interictal MEG could be substituted for ictal SPECT in epilepsy patients with TS; however, analysis of further similar cases is needed to confirm this.

Acknowledgment: We thank Ms. Kuniko Tsuchiya for excellent technical assistance. This study was supported in part by the Research Grant (17A-11) for Nervous and Mental Disorders from the Ministry of Health, Labour, and Welfare.

REFERENCES

1. Kotagal P. Epilepsy in the setting of neurocutaneous syndromes. In: Wyllie E, ed. *The Treatment of Epilepsy: Principles and Practice*. 3rd ed. Philadelphia: Lippincott Williams & Wilkins, 2001:627–636.
2. Rintahaka PJ, Chugani HT. Clinical role of positron emission tomography in children with tuberous sclerosis complex. *J Child Neurol* 1997;12:42–52.
3. Cheadle JP, Reeve MP, Sampson JR, et al. Molecular genetic advances in tuberous sclerosis. *Hum Genet* 2000;107:97–114
4. Chiron C, Dumas C, Jambaqué I, et al. Randomized trial comparing vigabatrin and hydrocortisone in infantile spasms due to tuberous sclerosis. *Epilepsy Res* 1997;26:389–395.
5. Bebin EM, Kelly PJ, Gomez MR. Surgical treatment for epilepsy in cerebral tuberous sclerosis. *Epilepsia* 1993;34:651–657.
6. Koh S, Jayakar P, Resnick T, et al. The localizing value of ictal SPECT in children with tuberous sclerosis complex and refractory partial epilepsy. *Epileptic Disord* 1999;1:41–46.
7. Avellino AM, Berger MS, Rostomily RC, et al. Surgical management and seizure outcome in patients with tuberous sclerosis. *J Neurosurg* 1997;87:391–396.
8. Guerreiro MM, Andermann F, Andermann E, et al. Surgical treatment of epilepsy in tuberous sclerosis: strategies and results in 18 patients. *Neurology* 1998;51:1263–1269.
9. Peresson M, Lopez L, Narici L, et al. Magnetic source imaging and reactivity to rhythmical stimulation in tuberous sclerosis. *Brain Dev* 1998;20: 512–518.
10. Kubota M, Ichiseki H, Takeshita K, et al. Magnetoencephalographic study of epileptic foci in patients with tuberous sclerosis. In: Yoshimoto T, Kotani M, Kuriki Set al., eds. *Recent Advances in Biomagnetism*. Sendai: Tohoku University Press, 1999:774–777.
11. Commission on Classification and Terminology of the International League Against Epilepsy. Proposal for revised classification of epilepsies and epileptic syndromes. *Epilepsia* 1989;30:389–399.
12. Minoshima S, Frey KA, Koeppe RA, et al. A diagnostic approach in Alzheimer's disease using three-dimensional stereotactic surface projections of Fluorine-18-FDG PET. *J Nucl Med* 1995;36:1238–1248.
13. O'Brien TJ, So EL, Mullan BP, et al. Subtraction ictal SPECT co-registered to MRI improves clinical usefulness of SPECT in localizing the surgical seizure focus. *Neurology* 1998;50:445–454.
14. Barkovich AJ. *Pediatric Neuroimaging*. 3rd ed. Philadelphia: Lippincott Williams & Wilkins, 2000.
15. Nixon JR, Miller GM, Okazaki H, et al. Cerebral tuberous sclerosis: postmortem magnetic resonance imaging and pathologic anatomy. *Mayo Clin Proc* 1989;64:305–311.

16. Curatolo P. Tuberous sclerosis: relationships between clinical and EEG findings and magnetic resonance imaging. In: Guerrini R, Andermann F, Canapicchi Ret al., eds. *Dysplasias of Cerebral Cortex and Epilepsy*. Philadelphia: Lippincott-Raven, 1996:191–198.
17. Romanelli P, Najjar S, Weiner HL, et al. Epilepsy surgery in tuberous sclerosis: multistage procedures with bilateral or multilobar foci. *J Child Neurol* 2002;17:689–692.
18. Curatolo P, Bombardieri R, Verdecchia M, et al. Intractable seizures in tuberous sclerosis complex: from molecular pathogenesis to the rationale for treatment. *J Child Neurol* 2005;20:318–325.
19. Morioka T, Nishio S, Ishibashi H, et al. Intrinsic epileptogenicity of focal cortical dysplasia as revealed by magnetoencephalography and electrocorticography. *Epilepsy Res* 1999;33:177–187.
20. Hader WJ, Mackay M, Otsubo H, et al. Cortical dysplastic lesions in children with intractable epilepsy: role of complete resection. *J Neurosurg Pediatr* 2004;100:110–117.
21. Bast T, Oezkan O, Rona S, et al. EEG and MEG source analysis of single and averaged interictal spikes reveals intrinsic epileptogenicity in focal cortical dysplasia. *Epilepsia* 2004;45:621–631.
22. Becker AJ, Urbach H, Scheffler B, et al. Focal cortical dysplasia of Taylor's balloon cell type: mutational analysis of the *TSC1* gene indicates a pathogenic relationship to tuberous sclerosis. *Ann Neurol* 2002;52:29–37.
23. Kameyama S, Fukuda M, Tomikawa M, et al. Surgical strategy and outcomes for epileptic patients with focal cortical dysplasia or dysembryoplastic neuroepithelial tumor. *Epilepsia* 2001;42(suppl 6):37–41
24. Bonte FJ, Devous MD Sr, Stokely EM, et al. Single-photon tomographic determination of regional cerebral blood flow in epilepsy. *AJNR Am J Neuroradiol* 1983;4:544–546.
25. Stefan H, Schneider S, Feistel H, et al. Ictal and interictal activity in partial epilepsy recorded with multichannel magnetoelectroencephalography: correlation of electroencephalography/electrocorticography, magnetic resonance imaging, single photon emission computed tomography, and positron emission tomography findings. *Epilepsia* 1992;33:874–887.

Cholesterol depletion facilitates ubiquitylation of NPC1 and its association with SKD1/Vps4

Yuki Ohsaki[1], Yuko Sugimoto[1], Michitaka Suzuki[1], Hiroshi Hosokawa[2], Tamotsu Yoshimori[3], Joanna P. Davies[4], Yiannis A. Ioannou[4], Marie T. Vanier[5], Kousaku Ohno[6] and Haruaki Ninomiya[1,*]

[1]Department of Neurobiology, Tottori University Faculty of Medicine, Yonago 683-8503, Japan
[2]Department of Intelligence Science and Technology, Graduate School of Informatics, Kyoto University, Kyoto 606-8501, Japan
[3]Department of Cell Genetics, National Institute of Genetics, Mishima 411-8540, Japan
[4]Department of Human Genetics, Mount Sinai School of Medicine, New York, NY 10029, USA
[5]INSERM Unit 189, Lyon-Sud Medical School and Fondation Gillet-Merieux, Lyon-Sud Hospital, 69921 Oullins, France
[6]Department of Child Neurology, Tottori University Faculty of Medicine, Yonago 683-8503, Japan
*Author for correspondence (e-mail: ninomiya@grape.med.tottori-u.ac.jp)

Accepted 23 March 2006
Journal of Cell Science 119, 2643-2653 Published by The Company of Biologists 2006
doi:10.1242/jcs.02993

Summary

Niemann-Pick disease type C (NPC) is an inherited lipid storage disorder caused by mutations in *NPC1* or *NPC2*. NPC1 is a polytopic glycoprotein that contains a sterol-sensing domain, whereas NPC2 is a soluble protein that contains an MD-2-like lipid-recognition domain. In the current study, we addressed the hypothesis that ubiquitylation of NPC1 might be regulated by cholesterol. We found that depletion of cellular cholesterol facilitated ubiquitylation of NPC1 expressed in COS cells. A loss-of-function mutant, NPC1(P691S), which contains an amino acid substitution in the sterol-sensing domain, failed to respond to cholesterol depletion. Another mutant, NPC1(δLLNF), which lacks the endosomal-targeting motif, also failed to respond. SKD1(E235Q), a dominant-negative mutant of SKD1/Vps4 that inhibits disassembly of the endosomal sorting complex required for transport (ESCRT), caused an accumulation of ubiquitylated NPC1. SKD1(E235Q) associated with NPC1 on the endosomal membrane, whereas wild-type SKD1 associated with NPC1 only when cells were depleted of cholesterol. Similarly, in control human skin fibroblasts, cholesterol depletion facilitated ubiquitylation of endogenous NPC1. In patient cells that lack NPC2 function, NPC1 was ubiquitylated regardless of cellular cholesterol levels, suggesting that NPC2 is required to prevent NPC1 ubiquitylation under cholesterol-rich conditions. These results suggest that ubiquitylation of NPC1 and its association with the ESCRT complex are controlled by endosomal cholesterol levels utilizing a mechanism that involves NPC2.

Key words: NPC1, NPC2, SKD1, Vps4, Ubiquitin, Cholesterol

Introduction

Niemann-Pick disease type C (NPC) is an autosomal recessive lipid storage disorder that is characterized by endosomal accumulation of low-density lipoprotein (LDL)-derived cholesterol (Patterson et al., 2001) and is caused by mutations in *NPC1* or *NPC2* (Carstea et al., 1997; Naureckiene et al., 2000). NPC1 is a membrane protein that resides primarily in the late endosome (Higgins et al., 1999), whereas NPC2 is a soluble protein that resides primarily in the lysosome (Vanier and Millat, 2004). These two proteins have been shown to function in the same endosomal cholesterol efflux pathway (Sleat et al., 2004). However, it is not clear how they interact with each other.

Solution of the human NPC1 membrane topology revealed a 1278 amino acid protein with 13 transmembrane domains and a sterol-sensing domain (SSD) located from transmembrane domains III to VII (Davies and Ioannou, 2000). Although this protein has been shown to possess a lipid permease activity (Davies et al., 2000) and the functional significance of its SSD has been well documented (Watari et al., 1999a; Millard et al., 2005), it is not known whether NPC1 function is regulated by cellular cholesterol. In addition to NPC1, SSDs are found in other proteins involved in the control of cellular cholesterol homeostasis: sterol regulatory element binding protein (SREBP) cleavage-activating protein (SCAP) and 3-hydroxy-3-methylglutaryl CoA reductase (HMG-CoAR), both of which reside primarily in the endoplasmic reticulum (ER). SCAP associates with the ER-retention proteins, Insig-1 and Insig-2, in a sterol-dependent manner: when cells are depleted of cholesterol, SCAP, together with SREBP, is released from the Insig proteins and transported to the Golgi apparatus, where a mature, active form of SREBP is generated by proteolysis and stimulates transcription of a diverse set of genes involved in cholesterol uptake and synthesis (Yang et al., 2002; Yabe et al., 2002). Similarly, HMG-CoAR associates with the Insig proteins in a sterol-dependent manner, but in this case, the association facilitates its ubiquitylation and subsequent degradation by the proteasome, thus shutting off endogenous cholesterol biosynthesis (Ravid et al., 2000; Sever et al., 2003a; Sever et al., 2003b). By analogy, one might hypothesize a cholesterol-dependent regulation of NPC1 function, either by its association with other proteins or by post-translational modifications.

Yeast genetic analysis has identified a number of proteins required for trafficking of endosomal proteins to the vacuole,

collectively termed the vacuolar protein sorting (Vps) proteins. These proteins assemble on the endosomal membrane to form the protein complexes ESCRT (endosomal sorting complex required for transport) -I, -II and -III, which operate sequentially (Katzmann et al., 2001; Babst et al., 2002a; Babst et al., 2002b). In this sorting process, ubiquitylation of an endosomal membrane protein serves as a signal for its sorting into the internal membranes of multivesicular bodies (Hicke, 2001). Vps4 is an ATPase that exists primarily in an inactive, ADP-bound cytosolic form and its active, ATP-bound form can transiently associate with the endosomal membrane. This protein is required for disassembly of the ESCRT-III. Expression of an ATPase-deficient, dominant-negative mutant of Vps4, the E233Q mutant, results in entrapment of ubiquitylated proteins on the endosomal membrane (Babst et al., 1997; Babst et al., 1998). Ncr1 is the yeast homolog of NPC1 and recent studies provided two lines of evidence that indicated a functional interaction between Ncr1 and Vps4. First, the targeting of Ncr1 to the vacuolar limiting membrane depends on Vps proteins, including Vps4 (Zhang et al., 2004). Second, Ncr1-null and Vps4-null cells share the same phenotype – resistance to the ether lipid drug edelfosine (Berger et al., 2005).

Mammalian counterparts to Vps proteins are presumed to function in a similar manner, and have been shown to be required for the ubiquitin-dependent, lysosomal transport of various membrane proteins, such as epidermal growth factor receptor (EGFR) (Bishop and Woodman, 2000; Bishop et al., 2002), G-protein-coupled receptors (Shenoy et al., 2001) and the cystic fibrosis transmembrane conductance regulator (Sharma et al., 2004). The suppressor of potassium transport growth defect protein 1, SKD1, is a mammalian ortholog of Vps4 and is a member of the *N*-ethylmaleimide-sensitive factor and AAA-type ATPase family (Scheuring et al., 2001). Like Vps4 in yeasts, SKD1 shuttles between an ADP-bound cytosolic form and an ATP-bound membrane-associated form. Also, similar to Vps(E233Q), SKD1(E235Q) lacks the ATPase activity and has a dominant-negative effect when expressed in mammalian cells. Expressed SKD1(E235Q) protein disrupts endosomal trafficking and localizes to aberrant endosomes (Yoshimori et al., 2000; Fujita et al., 2003).

Given the presence of an SSD, we hypothesized that NPC1 might be ubiquitylated by a cholesterol-dependent mechanism. Following confirmation that cellular cholesterol depletion facilitated NPC1 ubiquitylation, we pursued the hypothesis further that NPC1 interacts with the ESCRT complex.

Results

Cholesterol depletion facilitated ubiquitylation of NPC1 expressed in COS cells

NPC1 ubiquitylation was examined in COS cells transfected with Flag-NPC1 and myc/His_6-ubiquitin. 48 hours after transfection, cells were incubated either in cholesterol-rich medium [DMEM + 10% bovine calf serum (BCS)] or cholesterol-depleted medium [DMEM + 10% lipoprotein-deficient serum (LPDS)] supplemented with compactin and mevalonate. When cells were incubated in the cholesterol-depleted medium, the total cellular cholesterol level decreased in a time-dependent manner to reach ~60% of the control level at 12 hours. The cholesterol level was restored by supplementation with 20 μg/ml LDL (Fig. 1A). Expressed Flag-NPC1 was recovered by immunoprecipitation with anti-Flag M2 agarose and the products were analyzed by immunoblotting. As expected, Flag-NPC1 was detected in the immunoprecipitation products as a broad band between 150 and 250 kDa, as a result of its extensive glycosylation (Watari et al., 1999a). In addition, a band just below the top of the gel was often observed (for example, see Fig. 1E), which might represent an oligomerized form of the protein. Cholesterol depletion had little, if any, effect on the steady-state levels of the expressed proteins. However, probing with anti-myc revealed that cholesterol depletion caused conjugation of myc/His_6-ubiquitin to Flag-NPC1 (Fig. 1B). The positive signals were constantly detected at 6 hours and were sustained up to 24 hours. The conjugation was also demonstrated by metal affinity purification of myc/His_6-ubiquitin. Flag-NPC1 was detectable in the affinity purification products from cholesterol-depleted cells (Fig. 1C, left panel). Probing the affinity purification products with anti-myc showed no overall increase of ubiquitylated proteins in cholesterol-depleted cells (Fig. 1C, right panel). To see whether the ubiquitylation was caused by overexpression of ubiquitin molecules, cells were transfected only with Flag-NPC1 construct. Probing the anti-Flag immunoprecipitation products with anti-ubiquitin P4D1 revealed conjugation of endogenous ubiquitin to Flag-NPC1 in cells depleted of cholesterol (Fig. 1D).

Next, by using myc/His_6-ubiquitin co-expression, we examined whether cholesterol, instead of LDL, could suppress Flag-NPC1 ubiquitylation. Supplementation of the cholesterol-depleted medium with free cholesterol caused dose-dependent suppression of Flag-NPC1 ubiquitylation (Fig. 1E), suggesting that the ubiquitylation was a result primarily to cholesterol depletion.

To characterize Flag-NPC1 ubiquitylation further, we conducted two lines of experiments, first to examine effects of U18666A and second to examine detergent solubility of ubiquitylated Flag-NPC1. U18666A is a sterol derivative that has been shown to induce an NPC-like phenotype (Ko et al., 2001). To see whether this compound affected Flag-NPC1 ubiquitylation, transfected cells were incubated with 2 μg/ml U18666A for 12 hours. U18666A treatment at this concentration and duration caused endosomal cholesterol accumulation as revealed by filipin staining (data not shown) and, as reported previously (Sugimoto et al., 2001), an increase in the steady-state levels of expressed Flag-NPC1. Despite its effects on the steady-state levels, U18666A did not affect Flag-NPC1 ubiquitylation in cholesterol-rich medium nor did it suppress Flag-NPC1 ubiquitylation in cholesterol-depleted medium (Fig. 1F).

Cholesterol is the major constituent of raft microdomains and a part of NPC1 has been shown to associate with these domains (Garver et al., 2000). Therefore, it was possible that cholesterol depletion changed distribution of Flag-NPC1, which might lead to its ubiquitylation. To test this possibility, we examined the levels of Flag-NPC1 and its ubiquitylated form in 1% Triton X-100-soluble and Triton X-100-insoluble fractions, since raft microdomains are preferentially recovered in the insoluble fractions (Simons and Ikonen, 1997). Incubation for 6 hours in the cholesterol-depleted medium

reduced the level of Flag-NPC1 recovered from insoluble fractions. However, ubiquitylated Flag-NPC1 was recovered both from soluble and insoluble fractions (Fig. 1G). These data did not support the notion that Flag-NPC1 ubiquitylation was secondary to re-distribution of the protein between raft and non-raft membrane domains.

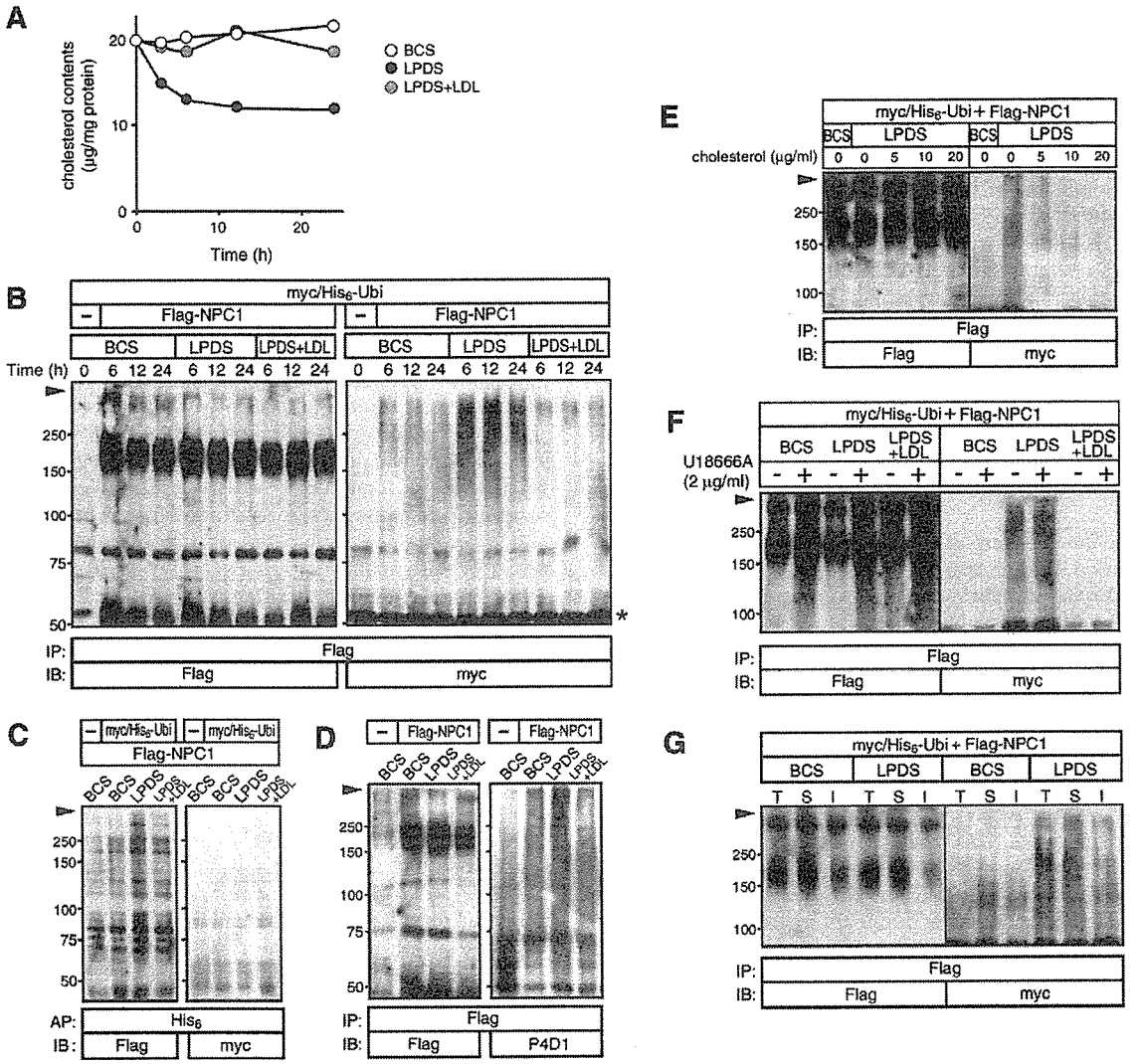

Fig. 1. Effects of cholesterol depletion on ubiquitylation of Flag-NPC1 expressed in COS cells. (A) Cellular cholesterol levels. Cells were cultured in cholesterol-rich medium (DMEM + 10% BCS) or cholesterol-depleted medium (DMEM + 10% LPDS supplemented with compactin and mevalonate) with or without LDL (20 μg/ml) up to 24 hours. Concentrations of total cholesterol in cell lysates were determined as described in the Materials and Methods. Each point represents the mean of duplicated determinations obtained in a single experiment. (B) Conjugation of myc/His_6-ubiquitin (myc/His_6-Ubi) to Flag-NPC1. Cells were transfected with expression constructs for myc/His_6-ubiquitin together with Flag-NPC1 or an empty vector. 48 hours after transfection, they were further cultured in the indicated medium. 0.5% CHAPS extracts were subjected to anti-Flag immunoprecipitation (IP) followed by immunoblotting (IB) with indicated antibodies. Molecular weights are given on the left (kDa). The arrowhead indicates the top of the separating gel and the asterisk indicates the heavy chain. (C) Co-purification of Flag-NPC1 with myc/His_6-ubiquitin. After incubation in the indicated medium for 6 hours, cell extracts were subjected to affinity purification with metal resin followed by immunoblotting with indicated antibodies. (D) Conjugation of endogenous ubiquitin to Flag-NPC1. Cells were transfected with Flag-NPC1 or an empty vector, cultured in the indicated medium for 6 hours and anti-Flag IP products were analyzed by indicated antibodies. (E) Effects of exogenous cholesterol on ubiquitylation of Flag-NPC1. Cells were transfected with myc/His_6-ubiquitin and Flag-NPC1, and cultured for 6 hours in cholesterol-rich or cholesterol-depleted medium supplemented with increasing concentrations of cholesterol. (F) Effects of U18666A. The transfected cells were cultured in the indicated medium for 12 hours in the presence or absence of U18666A. (G) Solubility of Flag-NPC1 to 1% Triton X-100. The transfected cells were cultured in the indicated medium for 6 hours. Total cell extracts (T), 1% Triton X-100-soluble (S) and Triton X-100-insoluble (I) fractions were prepared as described in the Materials and Methods. In E-G, anti-Flag immunoprecipitation products were subjected to immunoblotting with anti-Flag or anti-myc. All results shown are representative and were reproduced at least twice.

Mutant proteins Flag-NPC1(P691S) and Flag-NPC1(δLLNF) failed to respond to cholesterol depletion

To examine the role of the SSD in the cholesterol-level-dependent ubiquitylation, myc/His_6-ubiquitin co-expression experiments were repeated using Flag-NPC1(P691S), a loss-of-function mutant that contains an amino acid substitution in its SSD (Watari et al., 1999a; Millard et al., 2005). Anti-Flag immunoprecipitation products contained similar levels of Flag-NPC1 wild-type (wt) and P691S mutant proteins. Probing with anti-myc demonstrated that, in contrast to the wt protein, ubiquitylation of this mutant protein was barely facilitated following cholesterol depletion for 6 hours (Fig. 2A). To examine whether endosomal localization was required for NPC1 to undergo this modification, we examined effects of cholesterol depletion on the δLLNF mutant protein that lacks the C-terminal di-leucine motif and is retained in the ER (Watari et al., 1999b; Scott et al., 2004). As in the case of the P691S mutant, ubiquitylation of this mutant protein was barely affected by cholesterol depletion (Fig. 2B).

As a control experiment, we examined the effects of MG132, a proteasome inhibitor, on ubiquitylation of expressed proteins and found similar responses of the wt and mutant proteins. Similar to the wt protein, both P691S and δLLNF mutant proteins were extensively ubiquitylated in cells treated with 5 μM MG132 for 6 hours (Fig. 2).

Effects of MG132 and leupeptin on ubiquitylation of NPC1

Ubiquitylation can serve as a signal for protein degradation, which is executed by the cytosolic proteasome or by the lysosome. In an attempt to see whether ubiquitylated NPC1 underwent proteasomal and/or lysosomal degradation, we compared effects of MG132 and the lysosomal inhibitor leupeptin on Flag-NPC1 ubiquitylation. Treatment with 5 μM MG132 for 6 hours caused accumulation of ubiquitylated Flag-NPC1 and its effects were not influenced by cellular cholesterol levels. This increase in ubiquitylated Flag-NPC1 was accompanied by increased steady-state levels of Flag-NPC1, again regardless of the cholesterol levels (Fig. 3, upper panel). Similar results were reproduced with the proteasome inhibitor lactocystin (10 μM) (data not shown). By contrast, treatment with 100 μM leupeptin for 6 hours did not affect ubiquitylation of Flag-NPC1 either in cholesterol-rich or cholesterol-depleted conditions, nor caused appreciable changes in the steady-state levels of the protein (Fig. 3, lower panel). Incubation of the cells with NH_4Cl (10 mM for 6 hours) also failed to affect ubiquitylation of Flag-NPC1 and its steady-state levels (data not shown).

Interaction between SKD1(E235Q) and NPC1

Ubiquitylation can serve as a signal for the intracellular sorting of a protein. Since NPC1 resides primarily in the late endosome, we hypothesized that NPC1 was recognized by the ESCRT complex, which plays an essential role in the lysosomal sorting of ubiquitylated endosomal proteins. To address this hypothesis, NPC1 ubiquitylation was examined in the presence of SKD1(E235Q) (Fig. 4A), which inhibits disassembly of the ESCRT complex. When transfected cells were cultured in cholesterol-rich medium, expression of His_6-SKD1wt did not affect ubiquitylation of Flag-NPC1, whereas expression of His_6-SKD1(E235Q) caused a clear increase in the level of ubiquitylated Flag-NPC1 (Fig. 4B). Given its

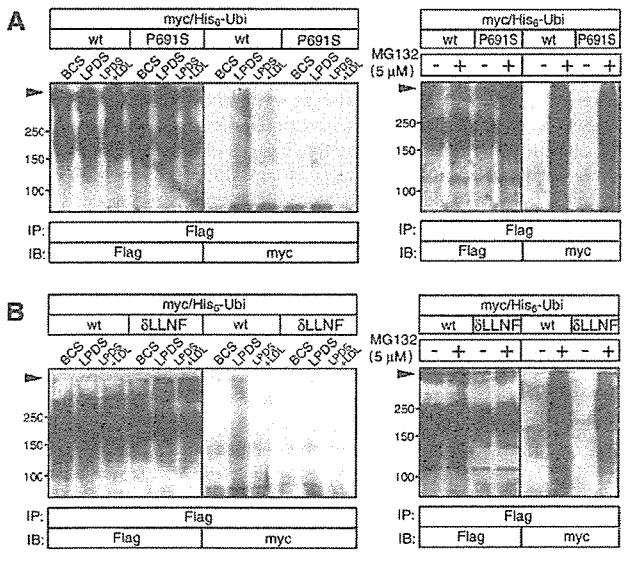

Fig. 2. Ubiquitylation of mutant NPC proteins. COS cells were transfected with myc/His_6-ubiquitin (myc/His_6-Ubi) together with Flag-NPC1 constructs that encoded the wild-type (wt) or mutant proteins P691S (A) or δLLNF (B); the arrowhead indicates the top of the separating gel. Cells were cultured in the indicated medium for 6 hours (left panels) or treated with or without MG132 for 6 hours (right panels). In both A and B, anti-Flag immunoprecipitation (IP) products were subjected to immunoblotting (IB) with anti-Flag or anti-myc. All results shown are representative and were reproduced at least twice.

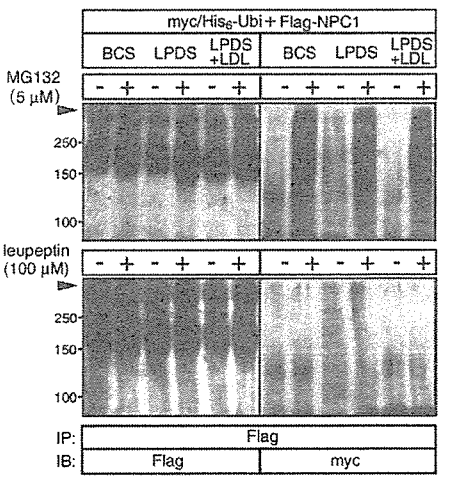

Fig. 3. Effects of MG132 and leupeptin on ubiquitylation of Flag-NPC1. COS cells were transfected with myc/His_6-ubiquitin (myc/His_6-Ubi) and Flag-NPC1 constructs, and were cultured in the indicated medium for 6 hours in the absence or presence of MG132 (upper panel) or leupeptin (lower panel); the arrowhead indicates the top of the separating gel. Anti-Flag immunoprecipitation (IP) products were subjected to immunoblotting (IB) with anti-Flag or anti-myc. All results shown are representative and were reproduced at least twice.

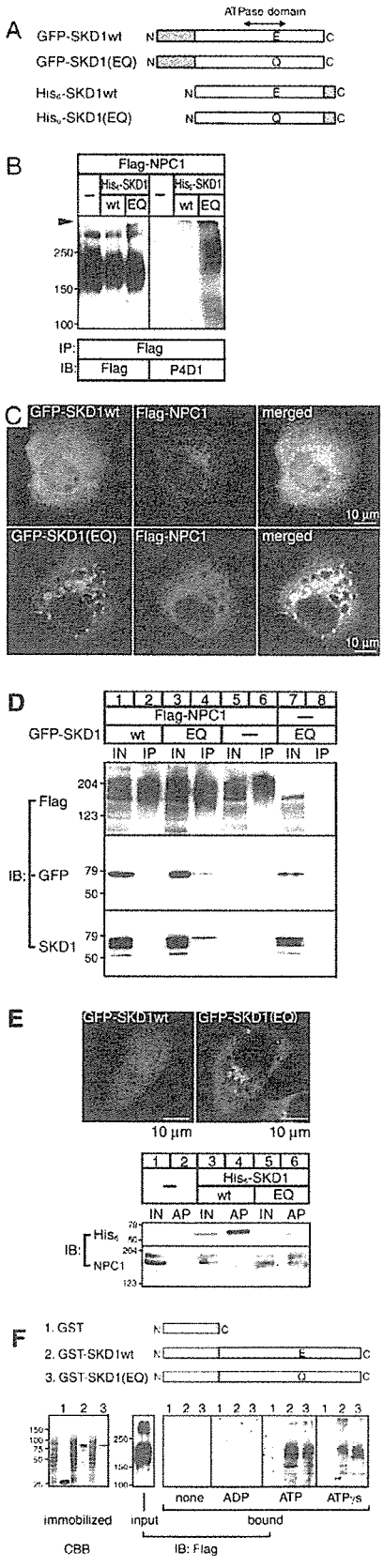

effects on NPC1 ubiquitylation, we examined whether SKD1(E235Q) co-localized and could interact with NPC1. Expression of a GFP-SKD1wt construct yielded a diffuse distribution in the cytoplasm and the nucleus, and did not induce any obvious changes of intracellular structures. Anti-Flag immunofluorescence revealed that Flag-NPC1 was retained in endosomes and did not co-localize with GFP-SKD1wt. As reported previously (Yoshimori et al., 2000; Fujita et al., 2003), expression of GFP-SKD1(E235Q) results in the formation of multiple aberrant vesicles that associated with the E235Q protein. Flag-NPC1 also localized to these aberrant endosomes and partially co-localized with GFP-SKD1(E235Q) (Fig. 4C). Detection of His_6-tagged SKD1 and Flag-NPC1 proteins yielded similar results (data not shown).

We next examined whether there was any interaction between Flag-NPC1 and SKD1 by immunoprecipitation and immunoblotting experiments. Similar levels of Flag-NPC1 were recovered by anti-Flag immunoprecipitation from cells expressing wt or E235Q mutant GFP-SKD1 protein (Fig. 4D, lanes 2 and 4). Probing the same immunoprecipitation products with anti-GFP showed that a portion of the GFP-SKD1(E235Q) protein was co-precipitated with Flag-NPC1

Fig. 4. Interaction between SKD1(E235Q) and NPC1. (A) Schematic representation of expressed SKD1 proteins. Each tag is shown in gray. (B) Flag-NPC1 ubiquitylation. COS cells were transfected with the Flag-NPC1 construct together with an empty vector or His_6-SKD1 constructs. 48 hours after transfection, anti-Flag immunoprecipitation (IP) products were subjected to immunoblotting (IB) with anti-Flag or anti-ubiquitin (P4D1). Molecular weights are given on the left (kDa); the arrowhead indicates the top of the separating gel. (C) Intracellular localization of GFP-SKD1 and Flag-NPC1. COS cells expressing Flag-NPC1 and GFP-SKD1 wild-type (wt; upper) or the E235Q mutant (EQ; lower) were fixed and stained with anti-Flag antibody. Bound antibody was visualized with Alexa Fluor 546-conjugated secondary antibody. Results shown are the representative images obtained with a confocal microscope. (D) Co-precipitation of Flag-NPC1 and GFP-SKD1 proteins. 0.5% CHAPS extracts were prepared from COS cells transfected with Flag-NPC1 together with GFP-SKD1wt or E235Q constructs. Anti-Flag immunoprecipitation products were analyzed by immunoblotting with the indicated antibodies. Cell extracts (IN: input) were loaded on lanes 1, 3, 5 and 7, and corresponding immunoprecipitation products were loaded on lanes 2, 4, 6 and 8. (E) Co-purification of endogenous NPC1 in CHO cells with His_6-SKD1 proteins. Upper; intracellular localization of GFP-SKD1. Results shown are the representative images obtained with a confocal microscope. Lower; affinity purification. 0.5% CHAPS extracts were prepared from cells transfected with an empty vector, His_6-SKD1wt or E235Q constructs. His_6-tagged proteins were affinity purified with metal affinity resin and were analyzed by immunoblotting with the indicated antibodies. Cell extracts (IN; input) were loaded on lanes 1, 3 and 5, and corresponding affinity-purification products (AP) were loaded on lanes 2, 4 and 6. (F) In vitro interaction between GST-SKD1 and Flag-NPC1. GST-fused proteins, as shown in the schematic representations, were expressed in *E. coli* and immobilized on glutathione sepharose (left, CBB: Coomassie Blue staining). 0.5% CHAPS extracts (input) were prepared from COS cells expressing Flag-NPC1. Cell extracts were incubated with immobilized GST-fused proteins in the absence or presence of 0.5 mM ADP, ATP or ATPγs. Bound proteins were eluted with glutathione and analyzed by anti-Flag immunoblotting (right). Molecular weights are given on the left (kDa). All results shown are representative and were reproduced at least twice.

(lane 4), whereas no GFP-SKD1wt could be co-precipitated (lane 2). These results were confirmed by probing with anti-SKD1 (lanes 2 and 4). Of note, in addition to GFP-SKD1 at 78 kDa, the anti-SKD1 antibody detected the endogenous SKD1 at 52 kDa (lanes 1, 3, 5 and 7), which, as expected, was not co-precipitated with Flag-NPC1 (lanes 2, 4 and 6). Further confirmation of the results was provided by repeating the above experiments using extracts from cells expressing His_6-tagged SKD1 proteins (data not shown).

Because CHO cells express a readily detectable level of NPC1 (Higaki et al., 2001), we used this cell line to test whether SKD1(E235Q) could interact with endogenous NPC1 (Fig. 4E). Unlike Flag-NPC1 expressed in COS cells, endogenous NPC1 in CHO cells exhibited relatively sharp bands with molecular weights of 170 and 200 kDa. Expression of GFP-SKD1(E235Q), but not GFP-SKD1, again caused the formation of aberrant endosomes containing the mutant protein. These results could be reproduced using His_6-tagged SKD1 proteins (data not shown). When the His_6-tagged SKD1 protein was affinity purified from cell extracts using metal affinity chromatography, a portion of endogenous NPC1 was co-purified with His_6-SKD1(E235Q) (Fig. 4E, lane 6), but not with His_6-SKD1wt (lane 4).

Although the above findings suggested an interaction between NPC1 and the ATP-bound, membrane-associated form of SKD1, it was possible that this interaction was secondary to the formation of the aberrant vesicles that are known to accumulate various endosomal proteins (Yoshimori et al., 2000; Fujita et al., 2003). To address this question, we examined whether NPC1 could bind to SKD1 in vitro (Fig. 4F). Human wt and E235Q mutant SKD1 proteins were expressed as GST-fusion proteins in *Escherichia coli*, whereas Flag-NPC1 was expressed and detergent solubilized from COS cells. GST-SKD1 proteins were immobilized on glutathione sepharose and incubated with 0.5% CHAPS-solubilized cell extracts. Flag-NPC1 bound to the sepharose with binding to both GST-SKD1wt and the E235Q mutant dependent on the presence of ATP or ATPγs. No binding could be detected in the presence of ADP.

Cholesterol depletion facilitated the interaction between NPC1 and wt SKD1

The above findings indicated that NPC1 could interact with the ATP-bound, membrane-associated form of SKD1. To address whether this interaction occurred in cholesterol-depleted cells, cells expressing Flag-NPC1 and His_6-SKD1wt were cultured in cholesterol-depleted medium. In these cells, there was an increase in the amount of His_6-SKD1wt that co-precipitated with Flag-NPC1, as compared with the level in cells cultured in cholesterol-rich medium (Fig. 5A). This co-precipitation was largely suppressed by LDL supplementation of cholesterol-depleted medium.

These findings suggested that at least a part of His_6-SKD1wt was recruited to the endosomes of cholesterol-depleted cells. To confirm this, Opti-prep fractionation of cell homogenates was carried out to detect the membrane-associated form of SKD1 (Fig. 5B). Following fractionation, the endosomal marker protein lamp2 was mainly distributed in fractions 4-7 and cholesterol depletion caused a leftward shift of this distribution to fractions 4-6. Similar to lamp2, Flag-NPC1 was distributed in fractions 3-8 and in 3-7 for the cholesterol-rich and cholesterol-depleted cell homogenates, respectively. Cholesterol depletion caused a more significant change in the distribution of His_6-SKD1wt. In cells cultured in cholesterol-rich medium, His_6-SKD1wt was exclusively recovered in the bottom fraction 12, whereas in cells cultured using cholesterol-depleted medium, this protein was also recovered in fractions

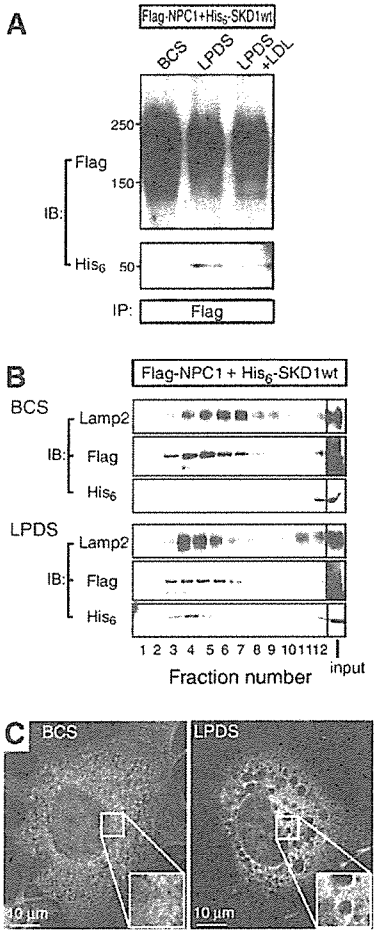

Fig. 5. Effects of cholesterol depletion on an interaction between Flag-NPC1 and wild-type SKD1. Transfected COS cells were cultured in cholesterol-rich or cholesterol-depleted medium with or without LDL for 16 hours. (A) Co-precipitation of His_6-SKD1wt with Flag-NPC1. Cells were transfected with His_6-SKD1wt together with Flag-NPC1 constructs. Anti-Flag immunoprecipitation (IP) products were analyzed by immunoblotting (IB) with the indicated antibodies. Molecular weights are given on the left (kDa). (B) Cell fractionation. Cells were transfected with Flag-NPC1 and His_6-SKD1wt constructs. Membrane fractions (100,000 *g* pellet) of cell homogenates were fractionated on an Opti-prep gradient. The fractions, together with the membrane fractions applied (input), were analyzed by immunoblotting with the indicated antibodies. Shown are representative results that were reproduced three times. (C) Intracellular localization of Flag-NPC1 and GFP-SKD1wt. Cells expressing Flag-NPC1 and GFP-SKD1wt were stained with anti-Flag antibody, and bound antibody was visualized with Alexa Fluor 546-conjugated secondary antibody. Results shown are the representative images obtained with a confocal microscope. Shown in the insets are the enlarged images of the indicated areas.

3-6. As a control experiment, we examined the distribution of His_6-SKD1(E235Q) and found that this protein was distributed in fractions 3-6 regardless of the cellular cholesterol levels (data not shown).

To confirm the endosomal recruitment of SKD1 in cholesterol-depleted cells further, we examined the intracellular localization of GFP-SKD1wt. As shown in Fig. 4C and Fig. 5C (left panel), when cells expressing Flag-NPC1 and GFP-SKD1wt were cultured in cholesterol-rich medium, GFP-SKD1wt was cytosolic and did not co-localize with endosomal Flag-NPC1. When these cells were cultured in cholesterol-depleted medium, GFP-SKD1wt was concentrated on the rim of enlarged endosomes where it co-localized with Flag-NPC1 (Fig. 5C, right panel).

Cholesterol depletion facilitated ubiquitylation of endogenous NPC1 and its association with SKD1 in controls but not in NPC human skin fibroblasts

The above findings indicated that cholesterol depletion induced ubiquitylation of NPC1 and its interaction with SKD1, when these proteins were expressed in COS cells. To examine whether cholesterol depletion had similar effects on endogenous NPC1 and SKD1, we used primary-cultured human skin fibroblasts from a control subject H34 and an NPC patient UCH (homozygous for the NPC1 H510P mutation). As reported previously (Yamamoto et al., 2000), UCH cells expressed undetectable levels of NPC1 (Fig. 6A), and were included as a negative control. Probing of H34 cell extracts with anti-NPC1 showed that, like CHO cells, these cells contained two species of NPC1 – a major band at 170 kDa and a minor band at 200 kDa – and that cholesterol depletion caused a marginal decrease in the steady-state levels of the NPC1 protein (Fig. 6A). Since immunoprecipitation of the endogenous NPC1 protein was unsuccessful, we employed anti-ubiquitin (P4D1) immunoprecipitation to evaluate the extent of NPC1 ubiquitylation (Fig. 6B). Probing with anti-NPC1 antibody showed that NPC1 was absent in the anti-ubiquitin immunoprecipitation products from cells cultured in cholesterol-rich medium, but was clearly detectable in the immunoprecipitation products from cells depleted of cholesterol. Probing of cell extracts with anti-ubiquitin antibody showed no overall increase of ubiquitylated proteins caused by cholesterol depletion (data not shown). The specificity of anti-NPC1 signals was confirmed by their absence in the immunoprecipitation products from UCH cells. Probing with anti-SKD1 antibody showed that cholesterol depletion increased the level of SKD1 contained in the anti-ubiquitin immunoprecipitation products from H34 cells. By contrast, cholesterol depletion did not alter the levels of SKD1 in the immunoprecipitation products from UCH cells.

Next, using Opti-prep fractionation, the recruitment of SKD1 to the endosomes of cholesterol-depleted cells was examined (Fig. 6C). Both lamp2 and NPC1 in membrane fractions of H34 cells were recovered in fractions 3-5 and, similar to the observations in COS cells (Fig. 5B), cholesterol depletion caused a leftward shift of this distribution to fractions 2 and 3. SKD1 was not recovered in these fractions when cells were cultured in cholesterol-rich medium, but was recovered in fractions 2 and 3 when cells were depleted of cholesterol.

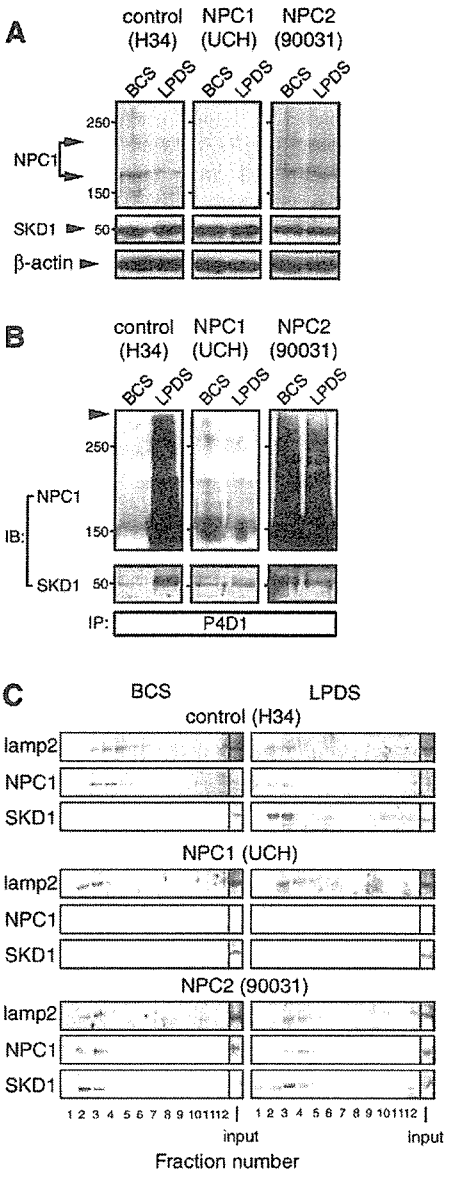

Fig. 6. Effects of cholesterol depletion on ubiquitylation of endogenous NPC1 and its interaction with SKD1 in human skin fibroblasts. Cells from a control subject or patients with NPC1 or NPC2 disease were cultured in cholesterol-rich or cholesterol-depleted medium for 16 hours. (A) Expression of NPC1 and SKD1. 0.5% CHAPS extracts were analyzed by immunoblotting (IB) with antibodies against the indicated proteins. (B) NPC1 ubiquitylation and its association with SKD1. 0.5% CHAPS extracts were subjected to anti-ubiquitin (P4D1) immunoprecipitation (IP) and the immunoprecipitated products were analyzed by immunoblotting with the indicated antibodies. Molecular weights are given on the left (kDa). (C) Cell fractionation. Membrane fractions (100,000 *g* pellet) of cell homogenates were fractionated on an Opti-prep gradient. All results shown are representative and were reproduced at least twice.

In membrane fractions of UCH cells, lamp2 was recovered in fractions 2 and 3 and, unlike in H34 cells, cholesterol depletion caused a rightward shift of this distribution to fractions 3-5. As